Published in final edited form as:
Geobiology. 2020 May ; 18(3): 326–347. doi:10.1111/gbi.12378.

Free and kerogen-bound biomarkers from late Tonian sedimentary rocks record abundant eukaryotes in mid-Neoproterozoic marine communities

J. Alex Zumberge[1], **Don Rocher**[2], **Gordon D. Love**[1]

[1]Department of Earth and Planetary Sciences, University of California, Riverside, CA, USA

[2]GeoMark Research, Houston, TX, USA

Abstract

Lipid biomarker assemblages preserved within the bitumen and kerogen phases of sedimentary rocks from the ca. 780–729 Ma Chuar and Visingsö Groups facilitate paleoenvironmental reconstructions and reveal fundamental aspects of emerging mid-Neoproterozoic marine communities. The Chuar and Visingsö Groups were deposited offshore of two distinct paleocontinents (Laurentia and Baltica, respectively) during the Tonian Period, and the rock samples used had not undergone excessive metamorphism. The major polycyclic alkane biomarkers detected in the rock bitumens and kerogen hydropyrolysates consist of tricyclic terpanes, hopanes, methylhopanes, and steranes. Major features of the biomarker assemblages include detectable and significant contribution from eukaryotes, encompassing the first robust occurrences of *kerogen-bound* regular steranes from Tonian rocks, including 21-norcholestane, 27-norcholestane, cholestane, ergostane, and cryostane, along with a novel unidentified C_{30} sterane series from our least thermally mature Chuar Group samples. Appreciable values for the sterane/hopane (S/H) ratio are found for both the *free* and *kerogen-bound* biomarker pools for both the Chuar Group rocks (S/H between 0.09 and 1.26) and the Visingsö Group samples (S/H between 0.03 and 0.37). The more organic-rich rock samples generally yield higher S/H ratios than for organic-lean substrates, which suggests a marine nutrient control on eukaryotic abundance relative to bacteria. A C_{27} sterane (cholestane) predominance among total C_{26}–C_{30} steranes is a common feature found for all samples investigated, with lower amounts of C_{28} steranes (ergostane and crysotane) also present. No traces of known ancient C_{30} sterane compounds; including 24-isopropylcholestanes, 24-*n*-propylcholestanes, or 26-methylstigmastanes, are detectable in any of these pre-Sturtian rocks. These biomarker characteristics support the view that the Tonian Period was a key interval in the history of life on our planet since it marked the transition from a bacterially dominated marine biosphere to an ocean system which became progressively enriched with eukaryotes. The eukaryotic source organisms likely encompassed photosynthetic primary producers, marking a rise in red algae, and consumers in a revamped trophic structure predating the Sturtian glaciation.

Correspondence: Gordon D. Love, Department of Earth and Planetary Sciences, University of California, Riverside, CA 92521, USA., glove@ucr.edu.

Keywords

eukaryotes; HyPy; lipid biomarkers; Neoproterozoic; steranes

1 | INTRODUCTION

Lipid biomarker assemblages recovered from thermally well-preserved sedimentary rocks can help unravel the temporal dynamics associated with the protracted emergence, diversification, and ecological expansion of Eukarya across the Proterozoic Eon (2,500–541 Ma) and may be used to assess the quantitative impact of early eukaryotes within ancient marine communities (Brocks et al., 2005, 2015, 2017; Dutkiewicz, Volk, Ridley, & George, 2003; Gallagher et al., 2017; Isson et al., 2018; Love et al., 2009; Luo, George, Xu, & Zhong, 2016; Nguyen et al., 2019). The mid-Proterozoic (1,800–1,000 Ma) was characterized by a remarkably long period of biogeochemical, tectonic, and climatic stability, with marine community structures buffered by feedback operating within coupled nutrient–carbon cycles imposed on primary production in the surface ocean (Cole et al., 2016; Crockford et al., 2018; Hardisty et al., 2017; Holland, 2006; Lyons, Reinhard, & Planavsky, 2014; Ozaki, Reinhard, & Tajika, 2019; Planavsky et al., 2011, 2014; Poulton & Canfield, 2011). A transition to a world with elevated surface oxygenation and nutrients, capable of supporting a more complex and productive marine biosphere, likely occurred during the Neoproterozoic Era (1,000–541 Ma). This is supported by multiple lines of evidence for first-order perturbations in climatic and tectonic conditions (Evans, 2000; Hoffman et al., 2017; Hoffman, Kaufman, Halverson, & Schrag, 1998; Kuznetsov, Bekker, Ovchinnikova, Gorokhov, & Vasilyeva, 2017; Li et al., 2008; Li, Evans, & Halverson, 2013; Macdonald et al., 2010; Maloof et al., 2006; McKenzie, Hughes, Gill, & Myrow, 2014; Rooney et al., 2014), ocean-atmosphere redox (Canfield, 1998; Husson & Peters, 2017; Johnston et al., 2012; Kump, 2008; Laakso & Schrag, 2014; Lenton & Daines, 2017; Planavsky et al., 2014; Prince, Rainbird, & Wing, 2019; Shields-Zhou & Och, 2011; von Strandmann et al., 2015; Turner & Bekker, 2016), carbon and other element cycling (Ader et al., 2014; Bjerrum & Canfield, 2011; Canfield & Teske, 1996; Crockford et al., 2018, 2019; Fike, Grotzinger, Pratt, & Summons, 2006; Halverson, Hoffman, Schrag, Maloof, & Rice, 2005; Horton, 2015; Lenton, Boyle, Poulton, Shields-Zhou, & Butterfield, 2014; Logan, Hayes, Hieshima, & Summons, 1995; Marais, Strauss, Summons, & Hayes, 1992; McFadden et al., 2008; Ridgwell & Zeebe, 2005; Schrag, Higgins, Macdonald, & Johnston, 2013), and for biological innovations/radiations (Bosak et al., 2012; Bosak, Macdonald, Lahr, & Matys, 2011; Brocks et al., 2017; Butterfield, 2015; Falkowski et al., 2004; Knoll, 2014; Love et al., 2009; Porter, 2016; Porter & Knoll, 2000; Porter, Meisterfeld, & Knoll, 2003; Sperling & Stockey, 2018).

Consistent with this body of work, recent evidence from lipid biomarker assemblages suggests that primary productivity in Mesoproterozoic oceans (~1,640–1,000 Ma) was consistently dominated by communities rich in bacteria as revealed by a dearth of eukaryotic (4-desmethyl) sterane biomarkers below detection limits (Figure 1; Blumenberg, Thiel, Riegel, Kah, & Reitner, 2012; Brocks et al., 2005, 2015, 2017; Flannery & George, 2014; Gueneli et al., 2018; Isson et al., 2018; Luo, Hallmann, Xie, Ruan, & Summons, 2015;

Nguyen et al., 2019; Suslova, Parfenova, Saraev, & Nagovitsyn, 2017) prior to the first detection of extractable eukaryotic biomarkers in Neoproterozoic rocks appearing from ca. 800 Ma and younger (Brocks et al., 2017; Grosjean, Love, Stalvies, Fike, & Summons, 2009; Isson et al., 2018; Love et al., 2009; van Maldegem et al., 2019).

The emergence of unicellular eukaryotes in ancient marine environments during the middle Proterozoic between ca. 1,900 and 1,600 Ma (Betts et al., 2018; Lamb, Awramik, Chapman, & Zhu, 2009; Parfrey, Lahr, Knoll, & Katz, 2011) and their subsequent protracted ecological expansion progressively changed the composition of the Proterozoic biosphere profoundly. This unicellular radiation likely preceded the evolution of complex multicellular organisms (Erwin et al., 2011; Narbonne & Gehling, 2003; Sperling & Stockey, 2018) and the establishment of a global marine trophic structure encompassing both abundant eukaryotic producers and consumers. However, our understanding of the timing and nature of Proterozoic ecological shifts and the environmental and tectonic perturbations that sparked the expansion of eukaryotes in the marine realm is quite sparse due to a patchy record of microfossil and biomarker data, particularly during the Tonian Period (1,000–720 Ma). The resulting “temporal gap” of biomarker data for this time interval is partly due to a scarcity of thermally well-preserved strata suitable for molecular biomarker analyses in comparison with Ediacaran and younger rocks. Lipid biomarker assemblages, many rich in eukaryotic steroids likely recording a high abundance of eukaryotic phytoplankton, have been reported from rocks and oils that have undergone a mild thermal history from various Cryogenian–Ediacaran marine paleoenvironments (~660–541 Ma; Figure 1; and references therein). For perspective, it should be noted that many immature Late Ediacaran rocks from oligotrophic basins deposited across Baltica actually possess strong bacterially sourced biomarker assemblages with only low eukaryotic contributions (Pehr et al., 2018). This highlights significant heterogeneity within the Ediacaran global ocean, in terms of the marine biological communities and the nutrient balance which sustained these, from one region to another.

In this study, we investigated the composition of the diverse biomarker assemblages preserved in well-preserved Tonian rocks sampled from two different paleocontinents, Baltica and Laurentia (Figure 2), that were deposited between ca. 780 and 729 Ma. These strata capture a crucial interval of geological time: leading up to, but prior to, the onset of the Sturtian glaciation and predating the imminent appearance of Earth’s earliest animal biomarker evidence found in the Cryogenian Period (Brocks et al., 2015; Love et al., 2009; Zumberge et al., 2018). Outcrops from the Chuar Group (Grand Canyon, Arizona, USA) and the Visingsö Group (Sweden) were subjected to parallel analyses of the *free* and *bound* lipid biomarker assemblages recovered from the bitumen and kerogen phases of sedimentary organic matter, respectively (French et al., 2015; Love et al., 2009; Love, Snape, Carr, & Houghton, 1995).

Kerogen is an insoluble and immobile organic geopolymer, which quantitatively represents the most abundant organic matter pool found in the geosphere (Love et al., 1995). Kerogen typically comprises > 90 wt.% of sedimentary organic matter yet is not routinely analyzed by organic geochemists since it is a high molecular weight substrate and molecular fragments must first be generated from covalent bond cleavage to access this biomarker

pool. Analysis of both the *free* (solvent-extractable) and the *kerogen-bound* biomarker pools separately offers the considerable advantages of ground-truthing the free hydrocarbon biomarker data, identifying any exogenous contaminants, as well as accessing a far higher proportion of the biomarker record. Routine recovery and analysis of the *kerogen-bound* biomarkers was performed here via the tested method of continuous-flow hydropyrolysis (HyPy) on the solvent-extracted rock residues (Bishop, Love, McAulay, Snape, & Farrimond, 1998; Love et al., 1995, 2009; Love, McAulay, Snape, & Bishop, 1997; Meredith, Snape, & Love, 2015). HyPy of kerogen is a valuable approach for testing the syngenicity of biomarker compounds in Precambrian rocks (Love et al., 2009; Nguyen et al., 2019; Zumberge et al., 2018), and it was a key analytical strategy that verified that polycyclic biomarker alkanes previously reported from overmature Archean and early Proterozoic rocks were exogenous trace contaminants (French et al., 2015). Alternative analytical approaches that scrutinize for exogenous biomarker components include the comparison of the exterior versus interior rock bitumen portion (E/I) compositions, which have been successfully employed on rocks of this age (Brocks et al., 2015, 2017), although these methods can only recover biomarkers from the soluble organic matter phase (bitumen) and not from the kerogen.

Here, we present and discuss the implications of first combined *free* and *kerogen-bound* records obtained for mid-Neoproterozoic rocks obtained from two different marine paleoenvironmental locations deposited prior to the Sturtian glaciation. Our samples comprised some of the most attractive Tonian sedimentary rock targets yet garnered for lipid biomarker investigation based on their appreciable total organic carbon (TOC) contents, including samples containing >1 wt% TOC, and mainly low thermal maturation history that allows for good preservation of primary biomarker structural features.

2 | MATERIALS AND METHODS

2.1 | Sedimentary rock samples

Sedimentary rocks from the Chuar Group were obtained from GeoMark Research and have been described in detail elsewhere (Cook, 1991). Briefly, all Chuar rocks were taken from one of two outcrop locations: Nankoweap Butte or Sixtymile Canyon, and sampled from within the Upper Walcott Member of the Kwagunt Formation, Chuar Group, Grand Canyon, Arizona. The Chuar Group mainly consists of marine mudstone deposited in an intracratonic extensional basin with time-variable oxygenated and redox-stratified waters, with evidence of ferruginous bottom waters with a later development of possibly euxinic conditions as interpreted using carbon, sulfur, and iron geochemical proxies (Johnston et al., 2010; Lillis, 2016). The Sixtymile Canyon strata were found to have undergone a milder thermal burial history than those from Nankoweap Butte (see later). Our results show that there is an obvious thermal maturity gradient of considerable magnitude between the two sampled outcrop locations, consistent from both Rock-Eval pyrolysis parameters and molecular biomarker maturity assessment (Tables 1 and 2). The sedimentary rocks from the Sixtymile Canyon section are less thermally mature (around *peak* oil window maturity) and better suited for lipid biomarker investigation than rocks from the Nankoweap Butte section, which are designated as *late* oil window maturity. Recently, the age of the Upper Walcott Member

was reassessed using coupled radioisotopic Re–Os and U–Pb geochronology to yield a date of 729 ± 0.9 Ma (Rooney et al., 2018), which is notably younger than the previous assigned date of 742 ± 6 Ma (Karlstrom et al., 2000).

Outcrop samples from the Visingsö Group were collected from within the Upper Member from previously described sections/localities including Uppgranna, Girabäcken, and Boeryd (Pulsipher & Dehler, 2019; Samuelsson & Strauss, 1999; Vidal, 1976) along the southeastern shoreline of Lake Vättern in southcentral Sweden. Additionally, a new outcrop section was found and sampled, dubbed *Broken Nodule*, and we report the biomarker results from strata in this location for the first time in this study. The Upper Member (<580 m thick) succession was deposited in an intracratonic basin and consists mainly of carbonaceous shales, as used here, with subordinate beds of dolomite, sandstone, and phosphorite (shale with >15% apatite), and dolomite/phosphorite nodules (Pulsipher & Dehler, 2019). Thermal maturity parameters for our Visingsö Group outcrops reveal that all sampled sections/localities are of intermediate *early-middle* oil window maturity and therefore suitable for biomarker analysis (Tables 1 and 2). The Visingsö Group has been interpreted as being deposited in a shallow marine intertidal and subtidal shelf environment that experienced intermittent upwelling of nutrient rich waters with organic-rich shales and carbonates in the upper unit member (Knoll & Vidal, 1980; Moczydlowska, Pease, Willman, Wickstrom, & Agic, 2018; Samuelsson & Strauss, 1999; Vidal, 1976). The maximum depositional age of the Visingsö Group has been reported as 886 ± 9 Ma, constrained by detrital zircon U–Pb geochronology (Moczydlowska et al., 2018; Pulsipher & Dehler, 2019), while the minimum depositional age heavily relies on the biostratigraphic similarities of other temporally equivalent locations including the Chuar Group and the lower Mount Harper Group (Yukon, Canada), which were both deposited during the Tonian (Moczydlowska et al., 2018). The appearance and widespread distribution of vase-shaped microfossils (VSMs) within the Visingsö Group is consistent with a Tonian-age range of approx. 780–730 Ma (Moczydlowska et al., 2018; Mus & Moczydlowska, 2000; Porter & Knoll, 2000; Pulsipher & Dehler, 2019; Riedman, Porter, & Calver, 2018).

2.2 | Total organic carbon (TOC) contents and Rock-Eval pyrolysis parameters

Total organic carbon content determination was performed at GeoMark Research. Powdered rock samples were initially decarbonated by treatment with 1 M hydrochloric acid (HCl) for 2 hr. The samples were then rinsed with water and flushed through a filtration apparatus to remove any remaining acid. The powders were then dried in a low temperature oven (110°C) for a minimum of 4 hr and then weighed to determine the percent carbonate content based on mass loss. TOC content was then measured from combustion of the dry residues by heating to 1,200°C using a LECO C230 instrument (GeoMark Research) that was calibrated with standards of known carbon content. The carbon dioxide yield from combustion was measured by an IR cell.

Approximately 100 mg of washed, ground (to 60 mesh) rock samples were analyzed with a Rock-Eval II instrument using standard conditions at GeoMark Research. Measurements include S1: free bitumen content (mg HC/g rock); S2: remaining hydrocarbon generation potential mainly from labile kerogen (mg HC/g rock); T_{max}: temperature at maximum

evolution of S2 hydrocarbons (°C); and S3: carbon dioxide yield from organic carbon (mg CO_2/g rock). The data were generated by heating according to the following parameters S1: 300°C for 3 min and S2: 300–550°C ramping at 25°C/min, and then held at 550°C for 1 min. The Hydrogen Index (in mg/g TOC) was calculated from: [(S2 × 100)/TOC], with TOC expressed in units of wt.%. Instrument calibration was achieved using a rock standard performed after every 10 sample runs.

2.3 | Rock extraction and bitumen fractionation

Solvent extraction of rock powders and subsequent separation of the rock bitumens was performed using established procedures (Haddad et al., 2016; Pehr et al., 2018; Rohrssen, Gill, & Love, 2015). Rock outcrop samples were carefully trimmed with a clean rock saw blade to remove the outer portion of the rock (typically 1–3 cm thickness) to isolate the inner rock portion for biomarker analyses and to minimize potential sources of exogenous organic contamination. The saw blade was extensively cleaned with a stepwise sequential solvent wash of hexane, dichloromethane (DCM), and methanol (MeOH) between samples. Trimmed rock pieces from inner portions were then sonicated in sequence with ultrapure water, MeOH, DCM, and hexane as described previously (Haddad et al., 2016). A SPEX 8515 shatterbox and a zirconia ceramic puck mill were used to powder the inner portion rock cuttings. Between each powdering step, the ceramic puck mill was extensively cleaned with the above solvent rinse cycle and pre-combusted quartz sand (850°C overnight) was powdered between samples to eliminate cross-contamination. As an important study control, samples of combusted quartz sand powders were also collected for the later analytical steps and were run in parallel with the rock samples as full analytical procedural blanks.

Lipid biomarkers were exhaustively extracted in 9:1 v:v DCM:MeOH solvent from the rock powders (between ~1 and 5 g depending on TOC wt.%.) using a Microwave Accelerated Reaction System (MARS; CEM Corp.) at 100°C for 15 min with constant stirring. Two sequential extractions were performed for each rock powder, and the extracts were combined after vacuum filtration at room temperature. After filtration, the extracted rock powder residue, containing kerogen as the principal sedimentary organic matter constituent, was collected and saved for subsequent continuous-flow hydrogen pyrolysis (HyPy) treatment. Laboratory procedural blanks using powdered combusted sand were extracted alongside each batch of rock powders to ensure that any background signals were negligible relative to the biomarker analytes recovered from the ancient rocks.

The bitumen (extract) was separated into aliphatic, aromatic, and polar fractions by silica gel column chromatography (36–70 mesh, activated at 450°C overnight). The aliphatic fraction was eluted with *n*-hexane, followed by the aromatic fraction with 1:1 v:v *n*-hexane:DCM, and finally, the polar fraction was eluted with 3:1 v:v DCM:MeOH. Aliphatic fractions, in this particular case, may also be correctly called *saturate* fractions for these bitumen extracts since these contain alkanes but no alkenes. However, we will use the broader term of *aliphatic* fraction throughout for the first product fraction which contains the hopanes, steranes, and other polycyclic alkane biomarkers. Elemental sulfur was removed from saturate fractions using (hydrochloric acid-activated and solvent-rinsed) copper pellets prior to biomarker analysis.

2.4 | Hydropyrolysis (HyPy) of extracted rocks

As well as a detailed investigation of the *free* (extractable) biomarker hydrocarbon assemblages, a sequential analysis of the *kerogen-bound* pool on a subset of rock samples was performed for comparison. The technique of hydropyrolysis (HyPy) involves heating samples in a stream of high pressure H_2 gas in a continuous-flow reactor configuration (Love et al., 1995). HyPy has been used previously to solubilize a significant fraction of sedimentary kerogen and other geomacromolecules, principally by cleavage of covalent cross-linkages (C–S, C–O, and C–C bonds) connecting the structural moieties together within the polymeric matrix. This fragmentation generates large quantities of soluble products and the release of the covalently bound lipid biomarkers in hydrocarbon form from the macromolecular matrix of kerogen with minimal alteration to their structure and stereochemistry (Love et al., 1995; Meredith et al., 2015).

The HyPy procedure for extracted rocks and kerogen concentrates has been described in detail previously (French et al., 2015; Love et al., 1995, 2009; Zumberge et al., 2018). Briefly, extracted rock powders (~0.5–1.0 g) were secured in the HyPy reactor tube atop a steel wool ball, which was Soxhlet extracted (DCM for at least 48 hr) and then combusted (450°C, 2 hr) prior to use to ensure that no contaminants were introduced to the reactor tube. Full procedural HyPy blanks were conducted using combusted silica gel as a substrate in the reactor tube. Blank HyPy runs with the steel wool ball loaded in the reactor tube were run to verify that the batch of steel wool was free of contamination, as described in French et al. (2015). HyPy is a temperature programmed pyrolysis technique using two temperature ramps: ambient to 250°C at 100°C/min, immediately followed by 250–520°C at 8°C/min while maintaining constant hydrogen pressure of ~150 bar with a flow rate of 6 L/min. The pyrolysate product for each sample was adsorbed onto silica gel (36–70 mesh, activated at 450°C overnight) contained within a dry ice-cooled product trap. After each HyPy run, the silica gel containing the adsorbed pyrolysate product was fractionated into three fractions (aliphatics, aromatic, and polars) using the same silica gel column chromatography method as described above for the rock bitumens (see Section 2.3).

2.5 | Lipid biomarker analysis

2.5.1 | Multiple Reaction Monitoring-Gas Chromatography-Mass Spectrometry (MRM-GCMS) of aliphatic hydrocarbon fractions—

Aliphatic fractions isolated from the extracted bitumen and kerogen HyPy products were analyzed by MRM-GC-MS conducted at UCR on a Waters Autospec Premier mass spectrometer equipped with an Agilent 7890A gas chromatograph and DB-1MS-coated capillary column (60 m × 0.25 mm i.d., 0.25 μm film thickness) using He for carrier gas. Typically, one microliter of a hydrocarbon fraction dissolved in *n*-hexane was injected onto the GC column in splitless injection mode at 320°C. The GC temperature program consisted of an initial hold at 60°C for 2 min, heating to 150°C at 10°C/min followed by heating to 320°C at 3°C/min and a final hold for 22 min. Analyses were performed in electron impact (EI) mode, with an ionization energy of 70 eV and an accelerating voltage of 8 kV. MRM transitions for C_{27}–C_{35} hopanes, C_{31}–C_{36} methylhopanes, C_{21}–C_{22} and C_{26}–C_{30} steranes, C_{30} methylsteranes, C_{24} tetracyclic terpanes, and C_{19}–C_{26} tricyclic terpanes were routinely monitored with the method used.

Procedural blanks performed with combusted sand typically yielded <0.1 ng of individual hopane and sterane isomers per gram of sand substrate. Polycyclic biomarker alkane (tricyclic terpanes, hopanes, steranes, etc.) abundances were quantified by addition of a deuterated C_{29} sterane standard [d_4-αααR−24-ethylcholestane (20R)] to aliphatic hydrocarbon fractions and comparison of relative peak areas. In MRM analyses, this standard compound was detected using 404→221 Da ion transition. Cross talk of non-sterane signal in 414→217 Da ion chromatograms from C_{30} and C_{31} hopanes was <0.2% of 412→191 Da hopane signal [mainly 17α,21β(H)-hopane, which is resolvable from C_{30} steranes] and <1% of the 426→191 Da signal, respectively (Rohrssen et al., 2015).

Polycyclic biomarkers were quantified assuming equal mass spectral response factors between analytes and the d_4-C_{29}-αααR−24-ethylcholestane (20R) internal standard. Analytical errors for absolute yields of individual hopanes and steranes are estimated at ±30%. Average uncertainties in hopane and sterane biomarker ratios are ±8% as calculated from multiple analyses of alkane fractions prepared from AGSO and GeoMark Research standard oils.

2.5.2 | Full scan GC-MS of the aliphatic and aromatic hydrocarbon fractions

—Total ion chromatograms (TICs) for the aliphatic and aromatic fractions were generated by GC-MS in full scan mode over a mass range of 50–800 Da using an Agilent 7890A gas chromatograph coupled to an Agilent 5975C inert Mass Selective Detector (MSD). Samples were injected as hexane solutions in splitless injection mode with a programmable temperature vaporizing (PTV) inlet and using He as the carrier gas. The GC was equipped with a DB-1MS capillary column (60 m × 0.32 mm i.d., 0.25 μm film thickness). The GC oven was programmed from 60°C (2 min), ramped to 150°C at 20°C/min, then to 325°C at 2°C/min, and held at 325°C for 20 min.

2.5.3 | Gas Chromatography-Triple Quadrupole (QQQ)-Mass Spectrometry (GC-QQQ-MS) of the aliphatic hydrocarbon fractions—

GC-QQQ-MS was performed at GeoMark Research on an Agilent 7000A Triple Quad (QQQ) interfaced with an Agilent 7890A gas chromatograph equipped with a J&W Scientific DB-5MS+DG capillary column (60 m × 0.25 mm i.d., 0.25 μm film thickness, 10 m guard). Using He as carrier gas, the flow was programmed from 1.2 to 3.2 ml/min. The GC oven was programmed from 40°C (2 min) to 325°C (25.75 min) at 4°C/min. Samples were spiked with a mixture of 7 internal standards (Chiron Routine Biomarker Internal Standard Cocktail 1) and injected in cold splitless mode at 45°C with the injector temperature ramped at 700°C/min to 300°C. The MS source was operated in EI-mode at 300°C with ionization energy at −70 eV. The number of molecular ion to fragment transitions varied throughout the run; dwell time was adjusted as needed to produce 3.5 cycles/s.

3 | RESULTS AND DISCUSSION

3.1 | Total organic carbon (TOC) content and thermal maturity of sedimentary rock samples

Total organic carbon contents for our Chuar rock samples are among some of the highest reported in the literature to date (Brocks et al., 2015, 2017) for Tonian sedimentary rocks

(min = 3.54 wt.%, max = 5.61 wt.%, mean = 4.36 wt.%; Table 1). Rock-Eval pyrolysis assessment (HI values used in conjunction with T_{max} and TOC contents, Table 1) reveal that Chuar Group outcrop samples from the Nankoweap Butte section are *late* oil window thermal maturity, while outcrops from the Sixtymile Canyon section are less mature and fall near *peak* oil window. Rock-Eval S2 values reflect the high amounts of organic carbon covalently bound within the kerogen (min = 4.13, max = 7.39, mean = 4.51 mg HC/g rock), while decreasing hydrogen index (HI) values are found as expected at elevated thermal maturity for Nankoweap Butte samples (min = 64, max = 132, mean = 101 mg/g TOC; Table 1). This is confirmed by the molecular biomarker abundance profiles (Figures 3 and 4), which generate multiple thermally sensitive biomarker proxies that consistently reflect elevated maturity in both the *free* and *bound* biomarker pools for Nankoweap Butte section (Table 2). Therefore, thermal maturity differences between the four Chuar Group samples play a significant role in modifying the hopane and sterane distribution patterns, as reflected by diastereoisomer ratios that are sensitive to elevated levels of thermal stress (Table 2 and Figures 3 and 4, e.g., C_{19}–C_{26} tricyclics/C_{30} αβH, C_{29}Ts/αβH, depletion of C31–35 homohopanes through side chain cracking; Moldowan et al., 1991; Peters & Moldowan, 1991; Seifert & Moldowan, 1978; Zumberge, 1987).

The extract and HyPy hydrocarbon products from the Nankoweap Butte locality are strikingly more altered through burial maturation than the stratigraphically equivalent Sixtymile Canyon samples and, as a result, the structural and stereochemical features of the polycyclic biomarker alkane signals from this section are not as well preserved (Figures 3 and 4). For example, the most abundant hopane compound in Nankoweap Butte extracts is a C_{27} rearranged hopane (Ts), with the side chain completely lost through thermal cracking. Also, a strong depletion in hopane compound abundances with increasing carbon number (27 > 29 >> 30–35) is observed for Nankoweap Butte samples due to extensive side chain cleavage across the whole hopane series. The obvious thermal maturity gradient between the two sections is an important factor to consider when interpreting the biomarker profiles. Thus, the two samples from Sixtymile Canyon (SWE2 & SW4) host the most thermally well-preserved Chuar Group biomarker assemblages and are ideal candidates for source organismal and paleoenvironmental reconstruction because of the better preservation and a wider range of linear, branched, and polycyclic hydrocarbon biomarker structures.

Compared to the Chuar Group, the Visingsö Group samples in this study have generally lower TOC (min = 0.26 wt.%, max = 1.13 wt.%, mean = 0.52 wt.%; Table 1) contents but contain better thermally preserved sedimentary organic matter due to a milder thermal burial history. This sample maturity lies in a position between the *early* to *middle* oil window resulting in better preservation of the polycyclic hydrocarbon biomarkers, including steranes, hopanes, and their methylated homologues (Figures 3 and 4). Rock-Eval parameters for eight Visingsö Group outcrops from four distinct sections report low S2 values (min = 0.22, max = 2.54, mean = 0.79 mg HC/g rock) and a range of HI values (min = 60, max = 225, mean = 130 mg/g TOC; Table 1) mostly related to organic matter source inputs under low productivity environmental conditions that were not persistently reducing. The T_{max} values obtained from Visingsö Group are mainly lower than those measured for Chuar Group samples, reflecting the lower thermal maturity for the former set (Table 1), although organic facies (the balance of labile vs. more recalcitrant organic matter from

mixed sources) can also significantly influence this measurement. The *early–middle* oil window maturity position is generally in agreement with the suite of thermally sensitive biomarker ratios (Table 2, and see Section 3.2), including the lower total amount of C_{19}–C_{26} tricyclic terpanes relative to C_{30} αβ hopane (tricyclics/C_{30} αβH; min = 0.61, max = 2.69, mean = 1.51 for solvent extracts), the good preservation of homohopane side chains (Figure 3), and lower C29/30 hopane ratios (Figure 4). The combined sampling of Chuar and Visingsö Groups allows for a more complete picture of late Tonian marine biomarker assemblage variations.

3.2 | Lipid biomarker assemblages

3.2.1 | Composition of polycyclic alkane biomarker distributions—Systematic patterns within the total aliphatic hydrocarbon distributions (e.g., relative abundance of tricyclic terpanes, hopanes, and steranes) are evident when comparing samples from the Chuar and Visingsö Groups (Figures 3 and 4). Typically, identification and comparison of the relative abundances of the major polycyclic biomarker hydrocarbon constituents permits assessment of major source biota inputs, environmental conditions at the time of deposition, and the overall degree of thermal maturity due to the burial maturation history of the host strata. Thermal maturity differences can account for some of the systematic differences in biomarker distributions between Chuar and Visingsö Group samples, and this maturity offset must be factored into any interpretations. For example, samples from the Chuar Group typically have significantly higher abundances of tricyclic terpanes relative to hopanes, whereas the opposite is true for the less mature Visingsö Group, which is a commonly observed maturity effect for ancient sedimentary rocks (Figure 4 and Table 2). This is due, in part, to the release of more tricyclic terpanes relative to hopanes from the kerogen into the bitumen phase and their enhanced preservation at high levels of thermal maturity relative to hopanes (Neto, Restle, Trendel, Connan, & Albrecht, 1983). Even accounting for thermal maturity influences though, there are still some consistent similarities in biomarker characteristics found for these Chuar and Visingsö Group samples reflecting late Tonian-age commonalities. Some of the principal biomarker characteristics evident in the terpane and sterane distributions are discussed below.

3.2.2 | Sterane assemblages in the Chuar group—Sterane biomarker distributions recovered from the *free* and *kerogen-bound* phases of organic matter (Figure 5) via solvent extraction and HyPy treatment, respectively, reveal that C_{26} and C_{27} dia- and regular steranes collectively account for the majority of detectable steranes with a combined average of 94% of the total C_{26}–C_{30} steranes. The C_{26} sterane contributions are higher in abundance in the more mature samples and thus mainly represent thermal cracking products from catagenesis. The primary sterane carbon number distribution for the Chuar Group samples then is a C_{27} (cholestane) dominance.

The diasterane abundances (βαS and βαR isomers are labeled) relative to regular sterane isomers, for all sterane compounds detected, are negligibly low in abundance for the kerogen fragmentation products from HyPy than for the corresponding bitumen extracts (Figure 5), as expected for hydropyrolysate products containing a dominance of genuine *kerogen-bound* sterane signal (Love et al., 1995, 1997, 2009). Cryostane (26-methylcholestane), a

terminally methylated C_{28} sterane biomarker prominent in pre-Sturtian paleoenvironments (Adam, Schaeffer, & Brocks, 2018; Brocks et al., 2015, 2017; Vogel, Moldowan, & Zinniker, 2005), is found in all four Chuar rock bitumens and constitutes an average of 4% of the total C_{26}–C_{30} steranes detected (Table 2).

Contrary to a previous report of biomarker assemblages from Chuar Group sedimentary rocks (Brocks et al., 2015), we were able to detect and verify signals for ergostane (24-methylcholestane) in the rock bitumens from all samples, with a mean abundance of 4% of the total C_{26}–C_{30} steranes (Table 2). Ergostane is also readily detected in the lipid biomarker assemblages generated from fragmentation of kerogen from the two best thermally preserved samples, SWE2 and SW4 (Figure 6 and Table 2), which helps confirm the syngenicity of these steranes within the host rocks. Due to the elevated thermal maturity of the two samples from Nankoweap Butte locality (namely, samples 36 and 50), any ergostane and cryostane cleaved by HyPy treatment are likely below detection limits and so only C_{26} and C_{27} regular steranes are detected in these residual kerogen products. For the late oil window samples from Nankoweap Butte, quantification with a biomarker standard showed that 96% of the total detectable sterane pool resides in the *free* extract phase while only 4% is from the *kerogen-bound* component. The majority of the kerogen-bound sterane pool would have been released by covalent bond cleavage during catagenesis at this late stage of the oil window. The low absolute abundances of steranes in pyrolysates from very mature kerogen explains why only the most abundant individual steranes (norcholestanes and cholestanes) are detectable in HyPy products from the two most mature samples from the Nankoweap Butte locality.

Stigmastane (regular C_{29} sterane) was seemingly absent in both the *free* and *bound* phases from all four outcrop samples from the Chuar Group. This finding is consistent with previously published biomarker data from the Kwagunt Formation, and the absence of any known C_{29} sterane series seems to be an attribute common to pre-Sturtian sedimentary strata thus far, which have been selected for their appropriate thermal maturity and possess no significant contributions of organic contamination from younger/exogenous hydrocarbons (Brocks et al., 2015, 2017; Hoshino et al., 2017; Isson et al., 2018; Summons et al., 1988; Vogel et al., 2005).

Reported here for the first time, we identified a low abundance but robust occurrence of a new C_{30} sterane compound series (with all four geologic isomers evident; ααα*S*, αββ*R* αββ*S*, ααα*R* in increasing elution time order) in both samples from the Sixtymile Canyon locality (SWE2 & SW4). As a *free* hydrocarbon constituent of the rock bitumen, this unknown C_{30} sterane series comprises only ca. 1% of relative abundance of the total C_{26}–C_{30} sterane signal for both outcrops and its presence was confirmed as a syngenetic compound via recovery from the kerogen-bound products generated from HyPy in which it constitutes ca. 2% of the total detectable steranes (Figure 7; Table 2). Relative to the elution patterns of other C_{30} sterane compounds with known structures, including 24-*n*-propylcholestane (24-npc), 24-isopropylcholestane (24-ipc), and 26-methylstigmastane (26-mes; Love et al., 2009; McCaffrey et al., 1994; Moldowan, 1984; Zumberge et al., 2018), this series has a markedly longer retention time and this has been confirmed with two separate analytical techniques (MRM-GC-MS and GC-QQQ-MS) employing capillary gas

chromatographic separation with columns with different stationary phases (DB-1MS and DB-5MS). These features suggest a sterane structure with an extended side chain, most likely with all three additional carbon atoms (relative to the basic cholestane skeleton) found at the terminal C-26 and/or C-27 positions making it a possible C_{30} analogue of cryostane (26-methylcholestane). No 24-npc, 24-ipc, or 26-mes steranes are detectable in any of our Tonian rock extracts or kerogen hydropyrolysate products, consistent with previous work that these specific C_{30} steranes are only found in Cryogenian and younger rocks and oils (Zumberge et al., 2018).

Our current understanding of unconventional steroid biosynthetic pathways that modify and extend the steroid side chain usually points to Porifera, and especially the demosponge group, as plausible candidate parent organisms for such a derived C_{30} steroid structure given that terminally methylated steroids appear to have a deep origin within the demosponge clade (Zumberge et al., 2018). Parallel analysis of intact sterol precursors with their sterane derivatives produced directly from hydrogenation of biomass from extant taxa has proved to be a reliable method for the elucidation of C_{30} sterane compounds detected commonly and in abundance in Neoproterozoic–Cambrian rocks and oils (Zumberge et al., 2018). No corresponding sterol precursor compound(s) capable of generating this C_{30} sterane signal has been identified from any modern taxa to our knowledge, however, so we can only speculate on the origins of this sterane marker at this stage.

Based on the elution patterns of stable ancient regular (4-desmethyl) C_{30} steranes (Zumberge et al., 2018), the new C_{30} sterane series detected in our Chuar outcrops likely contains an extended side chain through successive terminal alkylation, with no substituents at the conventional C-24 position, although the precise structure cannot yet be elucidated. This unknown sterane compound may have been biogenically sourced (and, thus, is a primary signal) or, alternatively, it is a secondary product from diagenetic alteration of other primary steranes. A biological rather than diagenetic origin for this C_{30} sterane compound can be supported by a number of lines of evidence, including: (a) Sedimentary diagenesis would be expected to produce multiple (not just one) chromatographically resolvable C_{30} sterane series if three extra carbon atoms (added to a C_{27} precursor) were non-specifically added to the steryl side chain at different positions, and (b) this sterane compound is not apparently common in the ancient rock record. Additionally, it has been shown from a large suite of immature Ediacaran, Cambrian, and Ordovician rocks, with highly variable TOC contents (0.1%–18%) and preserving strong C_{29} sterane preferences, that any C_{30} steranes in these samples are only found at trace levels or below detection limits (Pehr et al., 2018; Rohrssen et al., 2015). This highlights that C_{30} steranes are very often insignificant biomarker constituents in Neoproterozoic and Paleozoic rocks and oils, arguing against a diagenetic origin.

3.2.3 | Sterane assemblages in the Visingsö Group—Some of the main features of the sterane distribution patterns from our eight Visingsö Group samples are strikingly similar to those reported in our Chuar Group samples, even though both locations were subject to different thermal histories and were deposited offshore of two different paleocontinents. Biomarker distributions from all four Visingsö outcrop sections show cholestanes dominating over other steranes but with appreciable amounts of norcholestanes,

ergostanes and cryostanes, while no stigmastanes or commonly detected C_{30} steranes (24-npc, 24-ipc or 26-mes) series are found (Figure 8). The relative abundances of diasteranes are extremely low compared to regular steranes in the kerogen HyPy products than for the corresponding bitumen extracts, which indicates that the HyPy products contain genuine kerogen-bound steranes (Love et al., 1995, 1997, 2009).

The confirmation of ergostane (24-methylcholestane) as a genuine biomarker constituent in Tonian sedimentary rock samples from both Chuar and Visingsö Groups is an important finding here since 24-alkylated steranes are only known from eukaryotes and cannot apparently be produced by bacteria (Wei, Yin, & Welander, 2016). While there are a few known bacterial species capable of making 4-desmethylsterols that would preserve as cholestane in the rock record, these do not possess alkylation at C-24 or other side chain positions (Summons, Bradley, Jahnke, & Waldbauer, 2006; Wei et al., 2016). Furthermore, the detection of ergostane and steranes other than cholestane also argues against eukaryotic source organismal inputs exclusively comprised of heterotrophic protists (Brocks et al., 2017). In any case, modern red algae biosynthesize sterol distributions that would generate similar sterane patterns with cholestane dominance (Kodner, Pearson, Summons, & Knoll, 2008; Patterson, 1971). Our interpretation then is that eukaryotic phytoplankton, particularly from red algal clades, likely made a significant source contribution to the total sterane biomarker pool during the late Tonian Period.

For the Visingsö Group samples, however, we do not detect the late-eluting unknown C_{30} sterane series that is found in the most thermally well-preserved Chuar samples from the Sixtymile Canyon outcrop locality (Figures 7 and 8; Table 2). This is potentially due to the difference in TOC contents between the two locations, with a lower average TOC content for samples from the Visingsö Group (mean = 0.52 wt.% while those from the Chuar Group were 4.36 wt.%) giving an overall reduction in absolute sterane signal abundance combined with greater cross talk, which makes the C_{30} steranes more difficult to detect, and/or, more likely, reflects primary differences in the contributing source biota and paleoenvironments between the two locations. While the search for this unknown late-eluting C_{30} sterane series should continue in other thermally well-preserved Neoproterozoic rocks, we could not confirm the presence of this new C_{30} sterane compound in any of our Visingsö Group samples.

3.2.4 | Other terpane biomarkers in the Chuar and Visingsö Groups—The distribution of tricyclic, tetracyclic, and pentacyclic terpanes (particularly hopanes) in our suite of Chuar and Visingsö Group outcrops reflects source organismal inputs as well as preservational controls from thermal maturity modification. For example, the maturity gradient between the Nankoweap Butte and Sixtymile Canyon section of our Chuar Group outcrops is clearly illustrated by numerous maturity-sensitive hopane and other terpane stereoisomer ratios; including the overall abundance of C_{19} to C_{26} tricyclic terpanes to C_{30} αβ-hopane (tricyclics/C_{30}αβH), the extent of hopane side chain cleavage, Ts/Tm isomer ratios from both C_{27} and C_{29} hopanes (C_{27} Ts/Tm, C_{29} Ts/αβH), and the relative abundance of C_{30} βα-hopane (moretane) to C_{30} αβ-hopane (C_{30}βαH/C_{30}αβH; Figures 3, 4, and 9 and Table 2). Conversely, the hopane isomer distributions from our Visingsö Group rocks generally show a lower maturity distribution than all of the Chuar samples, consistent with a

typical *early–middle* (but prior to *peak*) oil window maturity assessment from lower rearranged/regular compound ratios for both C_{27} and C_{29} hopanes (C_{27} Ts/Tm, C_{29}Ts/αβH), enhanced moretanes (from higher C_{30}βαH/C_{30}αβH ratios), and from a lack of excessive hopane side chain cracking (Figures 3, 4 and 9, Table 2).

In addition to the obvious contrast of thermal maturity levels from each location, our collection of Chuar and Visingsö Group rocks also shows some fundamental differences in certain source diagnostic triterpane biomarker ratios, including the relative abundance of gammacerane to C_{30} hopane (G/C_{30}αβH; Table 2). Specifically, the Chuar Group G/C_{30}αβH ratio ranges from 0.11 to 0.45 (mean = 0.24), while the Visingsö Group values range only from 0.01 to 0.07 (mean = 0.03). This averages approximately an order of magnitude difference between the two locations, which is not explainable by the maturation differences. Gammacerane is the diagenetic product of the lipid tetrahymanol, found in abundance in ciliates, and is also commonly associated with water column stratification and/or hypersaline marine depositional environments (Damsté et al., 1995). Therefore, the higher G/C_{30}αβH ratios for the Chuar Group samples are consistent with the notion that ciliates thrived more in this depositional setting, although bacterial and other eukaryotic sources of gammacerane are also known (Peters, Walters, & Moldowan, 2005; Takishita et al., 2017). Ciliates are a class of heterotrophic eukaryotic protists that are phylogenetically distinct from the abundant testate ameba (preserved as vase-shaped microfossils; VSMs) found within the Chuar Group and other late Tonian paleoenvironments (Porter & Knoll, 2000; Porter et al., 2003; Strauss, Rooney, Macdonald, Brandon, & Knoll, 2014). It should be noted that in relation to the diverse distribution of VSM species recovered from the Chuar Group (which is the only Tonian environment where the majority of known VSM species (n = 8) have been recovered), the Visingsö Group hosts less abundant VSM occurrences (Morais et al., 2019; Riedman et al., 2018). The lower VSM microfossil abundance and diversity, together with the substantially lower gammacerane content and lower S/H ratios, suggests that eukaryotic heterotrophy was possibly suppressed in the Visingsö paleoenvironments compared with the Chuar Group.

Biomarker evidence for abundant Neoproterozoic ciliates, and by inference a rise in bacterivorous herbivory by eukaryotic consumers, was previously proposed from the detection of elevated abundances of gammacerane (Summons et al., 1988). The earliest noticeable spike in gammacerane abundance relative to hopanes in the rock record above a low Mesoproterozoic background value is first observed in sedimentary strata from the Chuar Group (ca. 780–729 Ma), deposited prior to the Sturtian glaciation (Summons et al., 1988; van Maldegem et al., 2019). We confirm here the elevated gammacerane/hopane ratio (Table 2) for the first time using the kerogen-bound biomarker pool from Walcott Member of the Chuar Group generated from HyPy analysis. Alternatively, other low-oxygen-adapted eukaryotes (Takishita et al., 2017) or certain bacteria (Peters et al., 2005) are also plausible sources of gammacerane (and methylgammaceranes). These alternative sources could explain the trace finite amounts of gammacerane detected in Mesoproterozoic rocks from the Roper Group (Nguyen et al., 2019). The polycyclic terpane biomarker assemblages are likely indicative of late Tonian marine communities, which locally could be rich in eukaryotic organisms, including eukaryotic primary producers and consumers, and which

were substantially different to the bacterially dominated communities supported in Mesoproterozoic ocean systems.

3.2.5 | Sterane/hopane ratios, sterane patterns, and their ecological significance—Time-resolved biomarker records compiled from successions of Proterozoic and Phanerozoic sedimentary rocks of appropriate thermal maturity often compare the relative abundances of hopane and sterane biomarkers as an insightful proxy for tracking the respective source organismal inputs from the domains Bacteria and Eukarya, respectively (Brocks et al., 2017; Grantham & Wakefield, 1988; Love et al., 2009; Schwark & Empt, 2006; Summons & Walter, 1990). The basis of this application comes from the knowledge garnered from decades of microbial lipid surveys coupled with extensive genomic data, which have shown that hopanoid and steroid lipids are synthesized in abundance by a broad and diverse range of bacteria and eukaryotes, respectively (Gold et al., 2016; Kodner et al., 2008; Summons et al., 2006), and since these possess similar long-term preservation potential.

The abundance ratio of the major (C_{27}–C_{35}) hopanes to (C_{27}–C_{29}) regular steranes provides a direct and informative measure of the relative contributions of bacteria and eukaryotes to sedimentary organic matter, which has proved useful to track the evolving Proterozoic surface ocean ecology. A temporal step change occurs as sterane/hopane (S/H) ratios shift from values of approximately zero (0.00) throughout the Paleoproterozoic and Mesoproterozoic as revealed by a dearth of eukaryotic steranes (Blumenberg et al., 2012; Brocks et al., 2005, 2015, 2017; Flannery & George, 2014; Gueneli et al., 2018; Isson et al., 2018; Luo et al., 2015; Nguyen et al., 2019; Suslova et al., 2017) before obviously increasing significantly during the Cryogenian and Ediacaran Periods (Brocks et al., 2017; Grosjean et al., 2009; Love et al., 2009; Stolper et al., 2017). In some cases, these can attain Phanerozoic average S/H range of ~0.5–2.0 for sedimentary rocks and oils, although bacterially dominated Ediacaran biomarker assemblages (with S/H values < 0.1) are also found in other locations and can feature for tens of millions of years (Pehr et al., 2018). As mentioned previously though, more biomarker data from sedimentary rocks that have undergone a mild thermal history are needed to assess the eukaryotic abundances in early-mid Neoproterozoic marine communities during this transition period, which is a principal focus of our study. Due to a deficiency of thermally well-preserved strata and paucity of biomarker data, far less is known about the temporal patterns and range of S/H and other lipid biomarker ratios across the Tonian Period (1,000–720 Ma). The Chuar and Visingsö Group samples used here help to fill this gap.

Eukaryotic sterane biomarkers first become detectable and commonly found in the late Tonian rock record, as verified by our detailed analysis of Chuar and Visingsö Group biomarker assemblages derived from both the bitumen and the kerogen organic phases. We generally attribute the scarcity of sterane biomarkers in strata older than ca. 800 Ma to a low overall ecological abundance of eukaryotes that inhabited the local settings rather than the complete absence of eukaryotes in these environments (Brocks et al., 2017; Isson et al., 2018; Nguyen et al., 2019). It is also possible that low-oxygen-adapted eukaryotes that did not possess 4-desmethylsterols may have been part of the community structure in marine settings older than ca. 800 Ma. Indeed, a few anaerobic protists have recently been shown to

lack sterols or sterol surrogates (such as tetrahymanol) in their cell membranes (Takishita et al., 2017), although the number of species that have been identified with this capability seems to be scarce and appears to be phylogenetically unrelated. Another possibility is that sterol biosynthesis did not actually evolve until during the mid-Neoproterozoic Era, but this scenario seems less likely, from molecular clock estimates that complex sterol synthesis was used by the ancestral crown-group eukaryote significantly prior to this (Gold, Caron, Fournier, & Summons, 2017) and from biomarker fossil evidence for older aromatized 4-methylsteroids, probably sourced from bacteria, from 1.64 Ga rocks from the Barney Creek Formation (Brocks et al., 2005).

Although microfossil (Javaux, Knoll, & Walter, 2001, 2004; Lamb et al., 2009) and molecular clock evidence suggests that unicellular stem eukaryotes had evolved by at least 1,900–1,600 Ma (Betts et al., 2018; King, 2004; Parfrey et al., 2011), the relative abundance of algal contributions to marine communities seems to have been suppressed with respect to bacteria in mid-Proterozoic marine settings. The ecological expansion of eukaryotes to become cosmopolitan and abundant in Proterozoic marine settings was hence a protracted process. This suppressed rise of microbial eukaryotes in marine environments may also have delayed the evolution of eukaryotic crown groups and complex multicellular eukaryotic organisms. The natural selection pressures operating within the marine biosphere would have changed as eukaryotic producers, and heterotrophs capable of ingesting those cells, became more prominent as members of marine communities.

In support of the emerging Proterozoic biomarker patterns, fossil evidence for diverse eukaryotic assemblages from multiple locations, including phytoplankton and heterotrophic protists, is also found in the early-mid Neoproterozoic from about 850 Ma and younger (Butterfield, Knoll, & Swett, 1994; Knoll, 2014; Knoll, Javaux, Hewitt, & Cohen, 2006; Morais et al., 2017; Porter & Knoll, 2000; Strauss et al., 2014). Microfossil analysis is best suited for detecting the earliest eukaryotes in the geological record, but it is difficult to use this approach to semi-quantitatively assess the eukaryotic abundance relative to bacterial source inputs and relative to the total sedimentary organic matter pool, since the dominant sedimentary organic matter component is amorphous kerogen. We look to the lipid biomarker record to try to better gauge the relative abundance of (regular steroid-synthesizing) eukaryotes versus bacterial source contributions in different Proterozoic marine settings.

Our approach to calculate S/H ratios is to include the most abundant compounds that account for a major fraction of the total detectable sterane pool in our samples, thus minimizing any overall biases from our dataset. The contributing compound peak areas for total steranes (S) include the main isomers (dia- and regular steranes) of C_{26}–C_{28} steranes (norcholestanes, cholestanes, ergostanes, cryostanes), as well as the newly detected but unknown C_{30} sterane series for the Sixtymile Canyon section samples from the Chuar Group. As previously described, regular C_{29} steranes (stigmastanes) and known C_{30} sterane compounds (24-npc/24-ipc/26-mes) are not detected in any of our Tonian samples so these are not used in our S/H ratio calculations. For the denominator “H” parameter, we use the dominant and most stable 17α,21β(H)-hopane series across the whole C_{27}–C_{35} carbon number range as described in detail in the footnote of Table 2. Brocks et al. (2017) only

included the main C_{27}–C_{29} sterane (regular and diasterane) isomers but excluded C_{26} (norcholestanes) and C_{28} sterane (cryostane) compounds in their ratio calculations. Neglecting the C_{26} (norcholestanes) may significantly underestimate S/H ratios in some samples as these compounds can account for a significant portion of the total detectable steranes (ca. 3%–40%; Table 2, affecting S/H ratios by close to a factor of two for the mature Chuar samples from the Nankoweap Butte section). Consideration of even shorter steranes, in the C_{19}–C_{25} range, produced from diagenetic and catagenetic alteration of primary steranes will also lead to significantly increased S/H ratios for high maturity rock and oil samples.

S/H values for the solvent-extractable phase from our two most thermally mature Chuar Group outcrops from the Nankoweap Butte section (outcrops 36 & 50) are 0.09 and 0.19, respectively, while those from the better thermally well-preserved Sixtymile Canyon section (outcrops SW4 & SWE2) are 0.38 and 0.37, respectively (Figure 10; Table 2). Corresponding values from the kerogen-bound pool are similar or higher (Table 2). Across the data set, the more organic-rich samples tend to have higher S/H ratios suggesting a nutrient-influenced productivity control on eukaryotic biota abundance (Figure 10). The two highly mature Chuar samples in our sample set likely fall off-trend (Figure 10) due to the organic constituents in these rocks having undergone more thermal alteration during their burial history, with increased side chain cracking and aromatization affecting the cumulative sterane (S) pool to a higher degree than the hopane (H) pool used for calculating S/H ratios. All eight of the outcrops from the Visingsö Group, sampled from four different sections and of *early* to *middle* oil window maturity, produced S/H values ranging from 0.03 to 0.36 (mean = 0.15; Figure 10; Table 2). The highest ratios of free S/H that we find for these Tonian rocks (up to ca. 0.4 for the solvent extracts) are similar in magnitude to the lower end of the typical range for organic-rich Phanerozoic rocks and oils (typically in the 0.5–2.0 range), suggesting abundant eukaryotic source contributions.

Brocks et al. (2017) concluded that “low” S/H values (0.003–0.42), in conjunction with a predominance of C_{27} steranes within the total sterane assemblage from multiple Tonian locations, reflects unique source contributions of unicellular heterotrophic eukaryotic protists but not from algae. Substantial contributions from eukaryotic phytoplankton could produce similar sterane carbon number patterns, however, since certain red algae biosynthesize predominantly C_{27} sterols with much lower amounts of C_{28} sterols (Kodner et al., 2008; Patterson, 1971), which reflects our sterane patterns. Indeed, a crown-group multicellular bangiophyte fossil derived from the red algal clade (Butterfield, 2000) has been found in rocks dated at ca. 1,050 Ma (Gibson et al., 2017). It should be noted also that Brocks et al. (2015) did detect ergostane (C_{28} regular sterane from a eukaryotic source) within the interior portion of one sample from the Girabäcken locality of the Visingsö Group (most equivalent to sample v19 in this study); however, they discounted this result since the same compound was not recovered from a collection of outcrop samples from the Chuar Group ($n = 9$). Overall, it is difficult to envisage how biomarker assemblages with appreciable S/H values in the 0.1–0.4 range can be attained without invoking significant eukaryotic primary producer inputs from photosynthetic algae, given the huge amounts of bacterial primary biomass and associated hopanoid lipid inputs to marine sedimentary environments at this time. A much larger amount of primary biomass at the base of a food

chain is required to support heterotrophs at higher trophic levels in any stable food web; so if ancient bacterial producers were making recalcitrant hopanoids, then it seemingly requires then that eukaryotic primary producers were also making sterols to obtain these appreciable S/H ratios.

A quantitatively significant component of the polycyclic biomarker assemblages detected from our Chuar and Visingsö Group sedimentary strata are composed of steranes, and our findings strongly suggest that abundant eukaryotic populations, probably including phytoplankton from red algal clades, emerged prior to the onset of the Sturtian glaciation. This purported Tonian algal rise is earlier than the Cryogenian algal expansion proposed by Brocks et al. (2017) but agrees with other evidence proposed for this timing obtained from zinc isotope records (Isson et al., 2018) and biogeochemical models (Feulner, Hallmann, & Kienert, 2015). While the assessment of when marine algae became globally “abundant” as primary producers is subjective and constantly being debated and revised (compare Brocks et al., 2017; Feulner et al., 2015; Isson et al., 2018; van Maldegem et al., 2019), the eukaryotic sterane biomarker records seemingly show an initial pulse of activity and notable abundance from ca. 800 Ma and onwards. This is approximately synchronous with observed volatility in Neoproterozoic carbon isotopic records (Halverson et al., 2005; Shields-Zhou & Och, 2011) and increases in the abundance and diversity of eukaryotic acritarchs and other fossils (Butterfield et al., 1994; Knoll, 2014; Knoll et al., 2006; Morais et al., 2017; Porter & Knoll, 2000; Strauss et al., 2014) along with striking changes in marine seawater chemistry, primary productivity and ocean redox conditions (Crockford et al., 2018, 2019; Isson et al., 2018; Kuznetsov et al., 2017; Lenton et al., 2014; Lenton & Daines, 2017; Turner & Bekker, 2016; von Strandmann et al., 2015), suggesting a more oxygenated and productive marine biosphere.

Thus, we perceive that the initial “rise of algae” occurred during the Tonian Period, as discerned from the common occurrence of regular steranes in conjunction with at least a two orders of magnitude rise in S/H compared with the Mesoproterozoic rock record (Figure 1). It was a later rise of green algae which prevailed during the Cryogenian Period, as evidenced from the switch from a C_{27} to a C_{29} sterane dominance (Brocks et al., 2017; Hoshino et al., 2017; Love et al., 2009). This green algal preference was sustained in the marine realm through the Ediacaran Period and through most of the Paleozoic Era. Note, this temporal pattern does not necessarily imply that red algae evolved before green algae, but rather that the prevailing marine environmental conditions and nutrient balance selected for certain groups of eukaryotes as the dominant primary producers through extended intervals of geological time (Grantham & Wakefield, 1988; Schwark & Empt, 2006).

4 | CONCLUSIONS

Lipid biomarker assemblages recovered from the *free* and *kerogen-bound* phases of sedimentary organic matter from thermally well-preserved rock samples from the 780–729 Ma Chuar and Visingsö Groups from Laurentia and Baltica, respectively, reveal convincing evidence for the proliferation of pre-Sturtian-age eukaryotic organisms. The ubiquity of regular sterane biomarkers and the sterane carbon number patterns with C_{27} steranes dominant in most samples (constituting up to 98% of total C_{26}–C_{30} steranes), but with

discernible amounts of C_{28} regular steranes (ergostane) also present, suggests that red algae were the dominant photosynthetic marine primary producers during the late Tonian Period. The principal characteristic features of the biomarker assemblages obtained from the solvent extract (*free*) phase were verified by parallel analysis of the *kerogen-bound* pool generated from HyPy, thus providing an important validation of the biomarker data.

We report here the oldest known occurrence of *kerogen-bound* regular sterane biomarkers generated from Precambrian sedimentary rocks. The C_{27} sterane (cholestane) dominance shows obvious similarities to the free sterane patterns reported previously for Tonian rocks but very different to the C_{29} (stigmastane) dominance found in some Cryogenian and most Ediacaran rocks deposited after the Sturtian glaciation. Along with cholestane, appreciable amounts of 27-norcholestanes (C_{26}), ergostanes (regular C_{28}), and cryostanes (unconventional C_{28}) are also found in most of our Tonian samples collected from both the Chuar and Visingsö Groups. The presence of regular C_{28} steranes (ergostanes) implies that the enzymatic capacity for alkylation at position C-24 on the steroid side chain was possible for eukaryotes in the Tonian Period, although the absence of any regular C_{29} steranes (stigmastanes) or conventional C_{30} steranes (24-npc and 24-ipc) suggests a more limited array of steroids synthesized by eukaryotes in marine environments prior to the Sturtian glaciation. We also found one novel resolvable C_{30} sterane compound present in some of the Chuar Group samples. This is possibly biogenic in origin, and the later GC elution time relative to known C_{30} sterane compounds suggests that it contains an unusual extended side chain. Any source assignment for this new ancient C_{30} sterane compound is tentative at this stage, however, until the precise side chain structure is confirmed.

While thermally immature Mesoproterozoic and older rocks consistently show no detectable eukaryotic sterane signal relative to hopanes (S/H ratios of <0.00), steranes become ubiquitous in mid-Neoproterozoic rocks, with S/H values of up to two orders of magnitude higher (up to 0.38 for the extractable bitumen and up to 1.26 for the kerogen-bound pool) from the Chuar and Visingsö Group samples used in this study. Such a significant temporal change in biomarker patterns is consistent with the concept of a fundamental global marine ecological upheaval as Proterozoic oceans transitioned from supporting bacterially dominated ecosystems to communities rich in eukaryotic primary producers and heterotrophic protists. The values for our S/H ratios are generally higher in the more organic-rich Tonian rocks compared with the organic-lean samples, suggesting a possible nutrient throttle control on marine eukaryotic proliferation. During the late Tonian Period, an ecological expansion of steroid-producing eukaryotes occurred in the ancient marine realm, which probably encompasses red algae as well as unicellular heterotrophs given the sterane carbon number patterns and substantial S/H ratios found. Thus, we provide compelling biomarker evidence here for a late Tonian rise of (red) algae in marine environments offshore of two separate paleocontinents, predating the Sturtian glaciation event.

ACKNOWLEDGMENTS

Funding support for this research investigation came from the NASA Astrobiology Institute Team for Alternative Earths (NNA15BB03A) and from a NASA Exobiology Award to GDL (grant number 80NSSC18K1085). We are extremely grateful to the Agouron Institute for their contribution toward the purchase of a Waters Premier Autospec instrument used for MRM-GC-MS biomarker analyses at UC Riverside.

Funding information

NASA Astrobiology Institute Team for Alternative Earths, Grant/Award Number: NNA15BB03A; NASA Exobiology Award, Grant/Award Number: 80NSSC18K1085

REFERENCES

Adam P, Schaeffer P, & Brocks JJ (2018). Synthesis of 26-methylcholestane and identification of cryostanes in mid-Neoproterozoic sediments. Organic Geochemistry, 115, 246–249. 10.1016/j.orggeochem.2017.11.006

Ader M, Sansjofre P, Halverson GP, Busigny V, Trindade RIF, Kunzmann M, & Nogueira ACR (2014). Ocean redox structure across the Late Neoproterozoic Oxygenation Event: A nitrogen isotope perspective. Earth and Planetary Science Letters, 396, 1–13. 10.1016/j.epsl.2014.03.042

Bengtson S, Sallstedt T, Belivanova V, & Whitehouse M (2017). Three-dimensional preservation of cellular and subcellular structures suggests 1.6 billion-year-old crown-group red algae. PLoS Biology, 15(3), e2000735 10.1371/journal.pbio.2000735 [PubMed: 28291791]

Betts HC, Puttick MN, Clark JW, Williams TA, Donoghue PCJ, & Pisani D (2018). Integrated genomic and fossil evidence illuminates life's early evolution and eukaryote origin. Nature Ecology & Evolution, 2(10), 1556–1562. 10.1038/s41559-018-0644-x [PubMed: 30127539]

Bhattacharya S, Dutta S, & Summons RE (2017). A distinctive biomarker assemblage in an Infracambrian oil and source rock from western India: Molecular signatures of eukaryotic sterols and prokaryotic carotenoids. Precambrian Research, 290, 101–112. 10.1016/j.precamres.2016.12.013

Bishop AN, Love GD, McAulay AD, Snape CE, & Farrimond P (1998). Release of kerogen-bound hopanoids by hydropyrolysis. Organic Geochemistry, 29(4), 989–1001. 10.1016/S0146-6380(98)00140-5

Bjerrum CJ, & Canfield DE (2011). Towards a quantitative understanding of the late Neoproterozoic carbon cycle. Proceedings of the National Academy of Sciences of the United States of America, 108(14), 5542–5547. 10.1073/pnas.1101755108 [PubMed: 21422280]

Blumenberg M, Thiel V, Riegel W, Kah LC, & Reitner J (2012). Biomarkers of black shales formed by microbial mats, Late Mesoproterozoic (1.1 Ga) Taoudeni Basin, Mauritania. Precambrian Research, 196, 113–127. 10.1016/j.precamres.2011.11.010

Bosak T, Lahr DJG, Pruss SB, Macdonald FA, Gooday AJ, Dalton L, & Matys ED (2012). Possible early foraminiferans in post-Sturtian (716–635 Ma) cap carbonates. Geology, 40(1), 67–70. 10.1130/G32535.1

Bosak T, Macdonald F, Lahr D, & Matys E (2011). Putative Cryogenian ciliates from Mongolia. Geology, 39(12), 1123–1126. 10.1130/G32384.1

Brocks JJ, Jarrett AJM, Sirantoine E, Hallmann C, Hoshino Y, & Liyanage T (2017). The rise of algae in Cryogenian oceans and the emergence of animals. Nature, 548(7669), 578–581. 10.1038/nature23457 [PubMed: 28813409]

Brocks JJ, Jarrett AJM, Sirantoine E, Kenig F, Moczydlowska M, Porter S, & Hope J (2015). Early sponges and toxic protists: Possible sources of cryostane, an age diagnostic biomarker antedating Sturtian Snowball Earth. Geobiology, 14(2), 129–149. 10.1111/gbi.12165 [PubMed: 26507690]

Brocks JJ, Love GD, Summons RE, Knoll AH, Logan GA, & Bowden SA (2005). Biomarker evidence for green and purple sulphur bacteria in a stratified Palaeoproterozoic sea. Nature, 437(7060), 866–870. 10.1038/nature04068 [PubMed: 16208367]

Butterfield NJ (2000). Bangiomorpha pubescens n. gen., n. sp.: implications for the evolution of sex, multicellularity, and the Mesoproterozoic/Neoproterozoic radiation of eukaryotes. Paleobiology, 26(3), 386–404. 10.1666/0094-8373(2000)026<0386:Bpngns>2.0.Co;2

Butterfield NJ (2015). The Neoproterozoic. Current Biology, 25(19), R859–R863. 10.1016/j.cub.2015.07.021 [PubMed: 26439347]

Butterfield NJ, Knoll AH, & Swett K (1994). Paleobiology of the Upper Proterozoic Svanbergfjellet Formation, Spitsbergen. Lethaia, 27(1), 76 10.1111/j.1502-3931.1994.tb01558.x

Canfield DE (1998). A new model for Proterozoic ocean chemistry. Nature, 396(6710), 450–453. 10.1038/24839

Canfield DE, & Teske A (1996). Late Proterozoic rise in atmospheric oxygen concentration inferred from phylogenetic and sulphur-isotope studies. Nature, 382(6587), 127–132. 10.1038/382127a0 [PubMed: 11536736]

Cole DB, Reinhard CT, Wang X, Gueguen B, Halverson GP, Gibson T, … Planavsky NJ (2016). A shale-hosted Cr isotope record of low atmospheric oxygen during the Proterozoic. Geology, 44(7), 555–558. 10.1130/G37787.1

Cook DA (1991). Sedimentology and shale petrology of the Upper Proterozoic Walcott Member, Kwagunt Formation, Chuar Group, Grand Canyon, Arizona. M.S. thesis, Northern Arizona University, Flagstaff, 128 p.

Crockford PW, Hayles JA, Bao H, Planavsky NJ, Bekker A, Fralick PW, … Wing BA (2018). Triple oxygen isotope evidence for limited mid-Proterozoic primary productivity. Nature, 559(7715), 613–616. 10.1038/s41586-018-0349-y [PubMed: 30022163]

Crockford PW, Kunzmann M, Bekker A, Hayles J, Bao H, Halverson GP, … Wing BA (2019). Claypool continued: Extending the isotopic record of sedimentary sulfate. Chemical Geology, 513, 200–225. 10.1016/j.chemgeo.2019.02.030

Damsté JSS, Kenig F, Koopmans MP, Koster J, Schouten S, Hayes JM, & Deleeuw JW (1995). Evidence for gammacerane as an indicator of water column stratification. Geochimica et Cosmochimica Acta, 59(9), 1895–1900. 10.1016/0016-7037(95)00073-9 [PubMed: 11540109]

Dutkiewicz A, Volk H, Ridley J, & George S (2003). Biomarkers, brines, and oil in the Mesoproterozoic, Roper Superbasin, Australia. Geology, 31(11), 981–984. 10.1130/G19754.1

Erwin DH, Laflamme M, Tweedt SM, Sperling EA, Pisani D, & Peterson KJ (2011). The Cambrian conundrum: Early divergence and later ecological success in the early history of animals. Science, 334(6059), 1091–1097. 10.1126/science.1206375 [PubMed: 22116879]

Evans DAD (2000). Stratigraphic, geochronological, and paleo-magnetic constraints upon the Neoproterozoic climatic paradox. American Journal of Science, 300(5), 347–433. 10.2475/ajs.300.5.347

Falkowski PG, Katz ME, Knoll AH, Quigg A, Raven JA, Schofield O, & Taylor FJR (2004). The evolution of modern eukaryotic phytoplankton. Science, 305(5682), 354–360. 10.1126/science.1095964 [PubMed: 15256663]

Feulner G, Hallmann C, & Kienert H (2015). Snowball cooling after algal rise. Nature Geoscience, 8(9), 659–662. 10.1038/ngeo2523

Fike DA, Grotzinger JP, Pratt LM, & Summons RE (2006). Oxidation of the Ediacaran ocean. Nature, 444(7120), 744–747. 10.1038/nature05345 [PubMed: 17151665]

Flannery EN, & George SC (2014). Assessing the syngeneity and indigeneity of hydrocarbons in the similar to 1.4 Ga Velkerri Formation, McArthur Basin, using slice experiments. Organic Geochemistry, 77, 115–125. 10.1016/j.orggeochem.2014.10.008

French KL, Hallmann C, Hope JM, Schoon PL, Zumberge JA, Hoshino Y, … Summons RE (2015). Reappraisal of hydrocarbon biomarkers in Archean rocks. Proceedings of the National Academy of Sciences of the United States of America, 112(19), 5915–5920. 10.1073/pnas.1419563112 [PubMed: 25918387]

Gallagher TM, Sheldon ND, Mauk JL, Petersen SV, Gueneli N, & Brocks JJ (2017). Constraining the thermal history of the North American Midcontinent Rift System using carbonate clumped isotopes and organic thermal maturity indices. Precambrian Research, 294, 53–66. 10.1016/j.precamres.2017.03.022

Gibson TM, Shih PM, Cumming VM, Fischer WW, Crockford PW, Hodgskiss MSW, … Halverson GP (2017). Precise age of *Bangiomorpha pubescens* dates the origin of eukaryotic photosynthesis. Geology, 46(2), 135–138. 10.1130/G39829.1

Gold DA, Caron A, Fournier G, & Summons RE (2017). Paleoproterozoic sterol biosynthesis and the rise of oxygen. Nature, 543, 420–423. 10.1038/nature21412 [PubMed: 28264195]

Gold DA, Grabenstatter J, de Mendoza A, Riesgo A, Ruiz-Trillo I, & Summons RE (2016). Sterol and genomic analyses validate the sponge biomarker hypothesis. Proceedings of the National Academy of Sciences of the United States of America, 113(10), 2684–2689. 10.1073/pnas.1512614113 [PubMed: 26903629]

Grantham PJ, & Wakefield LL (1988). Variations in the sterane carbon number distributions of marine source rock derived crude oils through geological time. Organic Geochemistry, 12(1), 61–73. 10.1016/0146-6380(88)90115-5

Grosjean E, Love GD, Stalvies C, Fike DA, & Summons RE (2009). Origin of petroleum in the Neoproterozoic-Cambrian South Oman Salt Basin. Organic Geochemistry, 40(1), 87–110. 10.1016/j.orggeochem.2008.09.011

Gueneli N, McKenna AM, Ohkouchi N, Boreham CJ, Beghin J, Javaux EJ, & Brocks JJ (2018). 1.1-billion-year-old porphyrins establish a marine ecosystem dominated by bacterial primary producers. Proceedings of the National Academy of Sciences of the United States of America, 115(30), E6978–E6986. 10.1073/pnas.1803866115 [PubMed: 29987033]

Haddad EE, Tuite ML, Martinez AM, Williford K, Boyer DL, Droser ML, & Love GD (2016). Lipid biomarker stratigraphic records through the Late Devonian Frasnian/Famennian boundary: Comparison of high-and low-latitude epicontinental marine settings. Organic Geochemistry, 98, 38–53. 10.1016/j.orggeochem.2016.05.007

Halverson GP, Hoffman PF, Schrag DP, Maloof AC, & Rice AHN (2005). Towards a Neoproterozoic composite carbon-isotope record. Geological Society of America Bulletin, 117, 1181–1207. 10.1130/B25630.1

Hardisty DS, Lu Z, Bekker A, Diamond CW, Gill BC, Jiang G, … Lyons TW (2017). Perspectives on Proterozoic surface ocean redox from iodine contents in ancient and recent carbonate. Earth and Planetary Science Letters, 463, 159–170. 10.1016/j.epsl.2017.01.032

Hoffman PF, Abbot DS, Ashkenazy Y, Benn DI, Brocks JJ, Cohen PA, … Warren SG (2017). Snowball Earth climate dynamics and Cryogenian geology-geobiology. Science Advances, 3(11), e1600983 10.1126/sciadv.1600983 [PubMed: 29134193]

Hoffman PF, Kaufman AJ, Halverson GP, & Schrag DP (1998). A Neoproterozoic snowball earth. Science, 281(5381), 1342–1346. 10.1126/science.281.5381.1342 [PubMed: 9721097]

Holland HD (2006). The oxygenation of the atmosphere and oceans. Philosophical Transactions of the Royal Society B-Biological Sciences, 361(1470), 903–915. 10.1098/rstb.2006.1838

Horton F (2015). Did phosphorus derived from the weathering of large igneous provinces fertilize the Neoproterozoic ocean? Geochemistry Geophysics Geosystems, 16(6), 1723–1738. 10.1002/2015gc005792

Hoshino Y, Poshibaeva A, Meredith W, Snape C, Poshibaev V, Versteegh GJM, … Hallmann C (2017). Cryogenian evolution of stigmasteroid biosynthesis. Science Advances, 3(9), e1700887 10.1126/sciadv.1700887 [PubMed: 28948220]

Husson JM, & Peters SE (2017). Atmospheric oxygenation driven by unsteady growth of the continental sedimentary reservoir. Earth and Planetary Science Letters, 460, 68–75. 10.1016/j.epsl.2016.12.012

Isson TT, Love GD, Dupont CL, Reinhard CT, Zumberge AJ, Asael D, … Planavsky NJ (2018). Tracking the rise of eukaryotes to ecological dominance with zinc isotopes. Geobiology, 16(4), 341–352. 10.1111/gbi.12289 [PubMed: 29869832]

Javaux EJ, Knoll AH, & Walter MR (2001). Morphological and ecological complexity in early eukaryotic ecosystems. Nature, 412(6842), 66–69. 10.1038/35083562 [PubMed: 11452306]

Javaux EJ, Knoll AH, & Walter MR (2004). TEM evidence for eukaryotic diversity in mid-Proterozoic oceans. Geobiology, 2(3), 121–132. 10.1111/j.1472-4677.2004.00027.x

Johnston DT, Poulton SW, Dehler C, Porter S, Husson J, Canfield DE, & Knoll AH (2010). An emerging picture of Neoproterozoic ocean chemistry: Insights from the Chuar Group, Grand Canyon, USA. Earth and Planetary Science Letters, 290(1–2), 64–73. 10.1016/j.epsl.2009.11.059

Johnston DT, Poulton SW, Goldberg T, Sergeev VN, Podkovyrov V, Vorob'eva NG, … Knoll AH (2012). Late Ediacaran redox stability and metazoan evolution. Earth and Planetary Science Letters, 335, 25–35. 10.1016/j.epsl.2012.05.010

Karlstrom KE, Bowring SA, Dehler CM, Knoll AH, Porter SM, Des Marais DJ, … Davidek KL (2000). Chuar Group of the Grand Canyon: Record of breakup of Rodinia, associated change in the global carbon cycle, and ecosystem expansion by 740 Ma. Geology, 28(7), 619–622. 10.1130/0091-7613(2000)028<0619:C-gotgc>2.3.Co;2 [PubMed: 11543503]

Kelly AE, Love GD, Zumberge JE, & Summons RE (2011). Hydrocarbon biomarkers of Neoproterozoic to Lower Cambrian oils from eastern Siberia. Organic Geochemistry, 42(6), 640–654. 10.1016/j.orggeochem.2011.03.028

King N (2004). The unicellular ancestry of animal development. Developmental Cell, 7(3), 313–325. 10.1016/j.devcel.2004.08.010 [PubMed: 15363407]

Knoll AH (2014). Paleobiological perspectives on early eukaryotic evolution. Cold Spring Harbor Perspectives in Biology, 6(1), a016121 10.1101/cshperspect.a016121 [PubMed: 24384569]

Knoll AH, Javaux EJ, Hewitt D, & Cohen P (2006). Eukaryotic organisms in Proterozoic oceans. Philosophical Transactions of the Royal Society B-Biological Sciences, 361(1470), 1023–1038. 10.1098/rstb.2006.1843

Knoll AH, & Vidal G (1980). Late Proterozoic vase-shaped microfossils from the Visingsö Beds, Sweden. Geologiska Föreningens i Stockholm Förhandlingar, 102(3), 207–211. 10.1080/11035898009455157

Kodner RB, Pearson A, Summons RE, & Knoll AH (2008). Sterols in red and green algae: Quantification, phylogeny, and relevance for the interpretation of geologic steranes. Geobiology, 6(4), 411–420. 10.1111/j.1472-4669.2008.00167.x [PubMed: 18624688]

Kump LR (2008). The rise of atmospheric oxygen. Nature, 451(7176), 277–278. 10.1038/nature06587 [PubMed: 18202642]

Kuznetsov AB, Bekker A, Ovchinnikova GV, Gorokhov IM, & Vasilyeva IM (2017). Unradiogenic strontium and moderate-amplitude carbon isotope variations in early Tonian seawater after the assembly of Rodinia and before the Bitter Springs Excursion. Precambrian Research, 298, 157–173. 10.1016/j.precamres.2017.06.011

Laakso TA, & Schrag DP (2014). Regulation of atmospheric oxygen during the Proterozoic. Earth and Planetary Science Letters, 388, 81–91. 10.1016/j.epsl.2013.11.049

Lamb DM, Awramik SM, Chapman DJ, & Zhu S (2009). Evidence for eukaryotic diversification in the ~1800 million-year-old Changzhougou Formation, North China. Precambrian Research, 173(1–4), 93–104. 10.1016/j.precamres.2009.05.005

Lenton TM, Boyle RA, Poulton SW, Shields-Zhou GA, & Butterfield NJ (2014). Co-evolution of eukaryotes and ocean oxygenation in the Neoproterozoic era. Nature Geoscience, 7(4), 257–265. 10.1038/ngeo2108

Lenton TM, & Daines SJ (2017). Biogeochemical Transformations in the History of the Ocean. Annual Review of Marine Science, 9(9), 31–58. 10.1146/annurev-marine-010816-060521

Li ZX, Bogdanova SV, Collins AS, Davidson A, De Waele B, Ernst RE, … Vernikovsky V (2008). Assembly, configuration, and break-up history of Rodinia: A synthesis. Precambrian Research, 160(1–2), 179–210. 10.1016/j.precamres.2007.04.021

Li ZX, Evans DAD, & Halverson GP (2013). Neoproterozoic glaciations in a revised global palaeogeography from the breakup of Rodinia to the assembly of Gondwanaland. Sedimentary Geology, 294, 219–232. 10.1016/j.sedgeo.2013.05.016

Lillis PG (2016). The Chuar Petroleum System, Arizona and Utah In Dolan MP, Higley DK, & Lillis PG (Eds.), Hydrocarbon source rocks in unconventional plays, Rocky Mountain Region. Denver, CO: The Rocky Mountain Association of Geologists.

Logan GA, Hayes JM, Hieshima GB, & Summons RE (1995). Terminal Proterozoic reorganization of biogeochemical cycles. Nature, 376(6535), 53–56. 10.1038/376053a0 [PubMed: 11536694]

Love GD, Grosjean E, Stalvies C, Fike DA, Grotzinger JP, Bradley AS, … Summons RE (2009). Fossil steroids record the appearance of Demospongiae during the Cryogenian period. Nature, 457(7230), 718–721. 10.1038/nature07673 [PubMed: 19194449]

Love GD, McAulay A, Snape CE, & Bishop AN (1997). Effect of process variables in catalytic hydropyrolysis on the release of covalently bound aliphatic hydrocarbons from sedimentary organic matter. Energy & Fuels, 11(3), 522–531. 10.1021/ef960194x

Love GD, Snape CE, Carr AD, & Houghton RC (1995). Release of covalently-bound alkane biomarkers in high yields from kerogen via catalytic hydropyrolysis. Organic Geochemistry, 23(10), 981–986. 10.1016/0146-6380(95)00075-5

Luo GM, Hallmann C, Xie SC, Ruan XY, & Summons RE (2015). Comparative microbial diversity and redox environments of black shale and stromatolite facies in the Mesoproterozoic Xiamaling formation. Geochimica Et Cosmochimica Acta, 151, 150–167. 10.1016/j.gca.2014.12.022

Luo QY, George SC, Xu YH, & Zhong NN (2016). Organic geochemical characteristics of the Mesoproterozoic Hongshuizhuang Formation from northern China: Implications for thermal maturity and biological sources. Organic Geochemistry, 99, 23–37. 10.1016/j.orggeochem.2016.05.004

Lyons TW, Reinhard CT, & Planavsky NJ (2014). The rise of oxygen in Earth's early ocean and atmosphere. Nature, 506(7488), 307–315. 10.1038/nature13068 [PubMed: 24553238]

Macdonald FA, Schmitz MD, Crowley JL, Roots CF, Jones DS, Maloof AC, … Schrag DP (2010). Calibrating the Cryogenian. Science, 327(5970), 1241–1243. 10.1126/science.1183325 [PubMed: 20203045]

Maloof AC, Halverson GP, Kirschvink JL, Schrag DP, Weiss BP, & Hoffman PF (2006). Combined paleomagnetic, isotopic, and stratigraphic evidence for true polar wander from the Neoproterozoic Akademikerbreen Group, Svalbard, Norway. Geological Society of America Bulletin, 118(9–10), 1099–1124. 10.1130/B25892.1

Marais DJD, Strauss H, Summons RE, & Hayes JM (1992). Carbon isotope evidence for the stepwise oxidation of the Proterozoic environment. Nature, 359(6396), 605–609. 10.1038/359605a0 [PubMed: 11536507]

McCaffrey MA, Moldowan JM, Lipton PA, Summons RE, Peters KE, Jeganathan A, & Watt DS (1994). Paleoenvironmental implications of novel C-30 steranes in Precambrian to Cenozoic Age petroleum and bitumen. Geochimica Et Cosmochimica Acta, 58(1), 529–532. 10.1016/0016-7037(94)90481-2

McFadden KA, Huang J, Chu X, Jiang G, Kaufman AJ, Zhou C, … Xiao S (2008). Pulsed oxidation and biological evolution in the Ediacaran Doushantuo Formation. Proceedings of the National Academy of Sciences of the United States of America, 105, 3197–3202. 10.1073/pnas.0708336105 [PubMed: 18299566]

McKenzie NR, Hughes NC, Gill BC, & Myrow PM (2014). Plate tectonic influences on Neoproterozoic-early Paleozoic climate and animal evolution. Geology, 42(2), 127–130. 10.1130/G34962.1

McKirdy DM, Webster LJ, Arouri KR, Grey K, & Gostin VA (2006). Contrasting sterane signatures in Neoproterozoic marine rocks of Australia before and after the Acraman asteroid impact. Organic Geochemistry, 37(2), 189–207. 10.1016/j.orggeochem.2005.09.005

Meredith W, Snape CE, & Love GD (2015). Development and use of catalytic hydropyrolysis (HyPy) as an analytical tool for organic geochemical applications In Grice K (Ed.), Principles and practice of analytical techniques in geosciences (vol. 4, pp. 171–208). Cambridge, UK: The Royal Society of Chemistry.

Moczydlowska M, Pease V, Willman S, Wickstrom L, & Agic H (2018). A Tonian age for the Visingso Group in Sweden constrained by detrital zircon dating and biochronology: Implications for evolutionary events. Geological Magazine, 155(5), 1175–1189. 10.1017/S0016756817000085

Moldowan JM (1984). C-30-steranes, novel markers for marine petroleums and sedimentary-rocks. Geochimica Et Cosmochimica Acta, 48(12), 2767–2768. 10.1016/0016-7037(84)90321-1

Moldowan JM, Lee CY, Watt DS, Jeganathan A, Slougui NE, & Gallegos EJ (1991). Analysis and occurrence of C26-steranes in petroleum and source rocks. Geochimica Et Cosmochimica Acta, 55(4), 1065–1081. 10.1016/0016-7037(91)90164-Z

Morais L, Fairchild TR, Lahr DJG, Rudnitzki ID, Schopf JW, Garcia AK, … Romero GR (2017). Carbonaceous and siliceous Neoproterozoic vase-shaped microfossils (Urucum Formation, Brazil) and the question of early protistan biomineralization. Journal of Paleontology, 91(3), 393–406. 10.1017/jpa.2017.16

Morais L, Lahr DJG, Rudnitzki ID, Freitas BT, Romero GR, Porter SM, … Fairchild TR (2019). Insights into vase-shaped microfossil diversity and Neoproterozoic biostratigraphy in light of recent Brazilian discoveries. Journal of Paleontology, 93(4), 612–627. 10.1017/jpa.2019.6

Mus MM, & Moczydlowska M (2000). Internal morphology and taphonomic history of the Neoproterozoic vase-shaped microfossils from the Visingso Group, Sweden. Norsk Geologisk Tidsskrift, 80(3), 213–228. 10.1080/002919600433751

Narbonne GM, & Gehling JG (2003). Life after snowball: The oldest complex Ediacaran fossils. Geology, 31(1), 27–30. 10.1130/0091-7613(2003)031<0027:Lastoc>2.0.Co;2

Neto FRA, Restle A, Trendel JM, Connan J, & Albrecht P (1983). Occurrence and formation of tricyclic and tetracyclic terpanes in sediments and petroleum In Bjorøy M (Ed.), Advances in organic geochemistry 1981 (pp. 659–667). Chichester, UK: Wiley.

Nguyen K, Love GD, Zumberge JA, Kelly AE, Owens JD, Rohrssen MK, … Lyons TW (2019). Absence of biomarker evidence for early eukaryotic life from the Mesoproterozoic Roper Group: Searching across a marine redox gradient in mid-Proterozoic habitability. Geobiology, 17(3), 247–260. 10.1111/gbi.12329 [PubMed: 30629323]

Ozaki K, Reinhard CT, & Tajika E (2019). A sluggish mid-Proterozoic biosphere and its effect on Earth's redox balance. Geobiology, 17(1), 3–11. 10.1111/gbi.12317 [PubMed: 30281196]

Parfrey LW, Lahr DJG, Knoll AH, & Katz LA (2011). Estimating the timing of early eukaryotic diversification with multigene molecular clocks. Proceedings of the National Academy of Sciences of the United States of America, 108(33), 13624–13629. 10.1073/pnas.1110633108 [PubMed: 21810989]

Patterson GW (1971). Distribution of sterols in algae. Lipids, 6(2), 120 10.1007/Bf02531327

Pehr K, Love GD, Kuznetsov A, Podkovyrov V, Junium CK, Shumlyanskyy L, … Bekker A (2018). Ediacara biota flourished in oligotrophic and bacterially dominated marine environments across Baltica. Nature Communications, 9, 1807 10.1038/s41467-018-04195-8

Peters KE, & Moldowan JM (1991). Effects of source, thermal maturity, and biodegradation on the distribution and isomerization of homohopanes in petroleum. Organic Geochemistry, 17(1), 47–61. 10.1016/0146-6380(91)90039-M

Peters KE, Walters CC, & Moldowan JM (2005). The Biomarker Guide. Cambridge, UK: Cambridge University Press.

Planavsky NJ, McGoldrick P, Scott CT, Li C, Reinhard CT, Kelly AE, … Lyons TW (2011). Widespread iron-rich conditions in the mid-Proterozoic ocean. Nature, 477(7365), 448–451. 10.1038/nature10327 [PubMed: 21900895]

Planavsky NJ, Reinhard CT, Wang X, Thomson D, McGoldrick P, Rainbird RH, … Lyons TW (2014). Low mid-Proterozoic atmospheric oxygen levels and the delayed rise of animals. Science, 346(6209), 635–638. 10.1126/science.1258410 [PubMed: 25359975]

Porter SM (2016). Tiny vampires in ancient seas: evidence for predation via perforation in fossils from the 780–740 million-year-old Chuar Group, Grand Canyon, USA. Proceedings of the Royal Society B-Biological Sciences, 283(1831), 20160221 10.1098/rspb.2016.0221

Porter SM, & Knoll AH (2000). Testate amoebae in the Neoproterozoic Era: Evidence from vase-shaped microfossils in the Chuar Group, Grand Canyon. Paleobiology, 26(3), 360–385. 10.1666/0094-8373(2000)026<0360:Taitne>2.0.Co;2

Porter SM, Meisterfeld R, & Knoll AH (2003). Vase-shaped microfossils from the Neoproterozoic Chuar Group, Grand Canyon: A classification guided by modern testate amoebae. Journal of Paleontology, 77(3), 409–429. 10.1666/0022-3360(2003)077<0409:Vmftnc>2.0.Co;2

Poulton SW, & Canfield DE (2011). Ferruginous conditions: A dominant feature of the ocean through earth's history. Elements, 7(2), 107–112. 10.2113/gselements.7.2.107

Prince JKG, Rainbird RH, & Wing BA (2019). Evaporite deposition in the mid-Neoproterozoic as a driver for changes in seawater chemistry and the biogeochemical cycle of sulfur. Geology, 47(4), 375–379. 10.1130/G45464.1

Pulsipher MA, & Dehler CM (2019). U-Pb detrital zircon geochronology, petrography, and synthesis of the middle Neoproterozoic Visingso Group, Southern Sweden. Precambrian Research, 320, 323–333. 10.1016/j.precamres.2018.11.011

Ridgwell A, & Zeebe RE (2005). The role of the global carbonate cycle in the regulation and evolution of the Earth system. Earth and Planetary Science Letters, 234(3–4), 299–315. 10.1016/j.epsl.2005.03.006

Riedman LA, Porter SM, & Calver CR (2018). Vase-shaped microfossil biostratigraphy with new data from Tasmania, Svalbard, Greenland, Sweden and the Yukon. Precambrian Research, 319, 19–36. 10.1016/j.precamres.2017.09.019

Rohrssen M, Gill BC, & Love GD (2015). Scarcity of the C-30 sterane biomarker, 24-n-propylcholestane, in Lower Paleozoic marine paleoenvironments. Organic Geochemistry, 80, 1–7. 10.1016/j.orggeochem.2014.11.008

Rooney AD, Austermann J, Smith EF, Li Y, Selby D, Dehler CM, … Macdonald FA (2018). Coupled Re-Os and U-Pb geochronology of the Tonian Chuar Group, Grand Canyon. Geological Society of America Bulletin, 130(7–8), 1085–1098. 10.1130/B31768.1

Rooney AD, Macdonald FA, Strauss JV, Dudas FO, Hallmann C, & Selby D (2014). Re-Os geochronology and coupled Os-Sr isotope constraints on the Sturtian snowball Earth. Proceedings of the National Academy of Sciences of the United States of America, 111(1), 51–56. 10.1073/pnas.1317266110 [PubMed: 24344274]

Samuelsson J, & Strauss H (1999). Stable carbon and oxygen isotope geochemistry of the upper Visingso Group (early Neoproterozoic), southern Sweden. Geological Magazine, 136(1), 63–73. 10.1017/S0016756899002253

Schrag DP, Higgins JA, Macdonald FA, & Johnston DT (2013). Authigenic carbonate and the history of the global carbon cycle. Science, 339(6119), 540–543. 10.1126/science.1229578 [PubMed: 23372007]

Schwark L, & Empt P (2006). Sterane biomarkers as indicators of Paleozoic algal evolution and extinction events. Palaeogeography, Palaeoclimatology, Palaeoecology, 240(1–2), 225–236. 10.1016/j.palaeo.2006.03.050

Seifert WK, & Moldowan JM (1978). Applications of steranes, terpanes and mono-aromatics to maturation, migration and source of crude oils. Geochimica Et Cosmochimica Acta, 42(1), 77–95. 10.1016/0016-7037(78)90219-3

Shields-Zhou G, & Och L (2011). The case for a Neoproterozoic oxygenation event: Geochemical evidence and biological consequences. GSA Today, 21(3), 4–11. 10.1130/GSATG102A.1

Sperling EA, & Stockey RG (2018). The temporal and environmental context of early animal evolution: Considering all the ingredients of an “explosion”. Integrative and Comparative Biology, 58(4), 605–622. 10.1093/icb/icy088 [PubMed: 30295813]

Stolper DA, Love GD, Bates S, Lyons TW, Young E, Sessions AL, & Grotzinger JP (2017). Paleoecology and paleoceanography of the Athel silicilyte, Ediacaran-Cambrian boundary, Sultanate of Oman. Geobiology, 15(3), 401–426. 10.1111/gbi.12236 [PubMed: 28387009]

Strauss JV, Rooney AD, Macdonald FA, Brandon AD, & Knoll AH (2014). 740 Ma vase-shaped microfossils from Yukon, Canada: Implications for Neoproterozoic chronology and biostratigraphy. Geology, 42(8), 659–662. 10.1130/G35736.1

Summons RE, Bradley AS, Jahnke LL, & Waldbauer JR (2006). Steroids, triterpenoids and molecular oxygen. Philosophical Transactions of the Royal Society B-Biological Sciences, 361(1470), 951–968. 10.1098/rstb.2006.1837

Summons RE, Brassell SC, Eglinton G, Evans E, Horodyski RJ, Robinson N, & Ward DM (1988). Distinctive hydrocarbon biomarkers from fossiliferous sediment of the Late Proterozoic Walcott Member, Chuar Group, Grand Canyon, Arizona. Geochimica Et Cosmochimica Acta, 52(11), 2625–2637. 10.1016/0016-7037(88)90031-2

Summons RE, & Walter MR (1990). Molecular fossils and microfossils of prokaryotes and protists from Proterozoic sediments. American Journal of Science, 290a, 212–244.

Suslova EA, Parfenova TM, Saraev SV, & Nagovitsyn KE (2017). Organic geochemistry of rocks of the Mesoproterozoic Malgin formation and their depositional environments (southeastern Siberian Platform). Russian Geology and Geophysics, 58(3–4), 516–528. 10.1016/j.rgg.2016.09.027

Takishita K, Chikaraishi Y, Tanifuji G, Ohkouchi N, Hashimoto T, Fujikura K, & Roger AJ (2017). Microbial eukaryotes that lack sterols. Journal of Eukaryotic Microbiology, 64(6), 897–900. 10.1111/jeu.12426 [PubMed: 28509379]

Turner EC, & Bekker A (2016). Thick sulfate evaporite accumulations marking a mid-Neoproterozoic oxygenation event (Ten Stone Formation, Northwest Territories, Canada). Geological Society of America Bulletin, 128(1–2), 203–222. 10.1130/B31268.1

van Maldegem LM, Sansjofre P, Weijers JWH, Wolkenstein K, Strother PK, Wormer L, … Hallmann C (2019). Bisnorgammacerane traces predatory pressure and the persistent rise of algal ecosystems after Snowball Earth. Nature Communications, 10, 476 10.1038/s41467-019-08306-x

Vidal G (1976). Late Precambrian microfossils from the Visingsö Beds in southern Sweden. Fossils and Strata, 9, 1–57.

Vogel MB, Moldowan JM, & Zinniker D (2005). Biomarkers from units in the Uinta Mountain and Chuar groups. Utah Geological Association Publication, 33, 75–96.

von Strandmann PAEP, Stueken EE, Elliott T, Poulton SW, Dehler CM, Canfield DE, & Catling DC (2015). Selenium isotope evidence for progressive oxidation of the Neoproterozoic biosphere. Nature Communications, 6, 10157 10.1038/ncomms10157

Wang XM, Zhao WZ, Zhang SC, Wang HJ, Su J, Canfield DE, & Hammarlund EU (2018). The aerobic diagenesis of Mesoproterozoic organic matter. Scientific Reports, 8, 13324 10.1038/s41598-018-31378-6 [PubMed: 30190572]

Wei JH, Yin XC, & Welander PV (2016). Sterol synthesis in diverse bacteria. Frontiers in Microbiology, 7, 990 10.3389/fmicb.2016.00990 [PubMed: 27446030]

Yang S, Kendall B, Lu XZ, Zhang FF, & Zheng W (2017). Uranium isotope compositions of mid-Proterozoic black shales: Evidence for an episode of increased ocean oxygenation at 1.36 Ga and evaluation of the effect of post-depositional hydrothermal fluid flow. Precambrian Research, 298, 187–201. 10.1016/j.precamres.2017.06.016

Zumberge JE (1987). Prediction of source rock characteristics based on terpane biomarkers in crude oils – A multivariate statistical approach. Geochimica Et Cosmochimica Acta, 51(6), 1625–1637. 10.1016/0016-7037(87)90343-7

Zumberge JA, Love GD, Cárdenas P, Sperling EA, Gunasekera S, Rohrssen M, … Summons RE (2018). Demosponge steroid biomarker 26-methylstigmastane provides evidence for Neoproterozoic animals. Nature Ecology & Evolution, 2(11), 1709–1714. 10.1038/s41559-018-0676-2 [PubMed: 30323207]

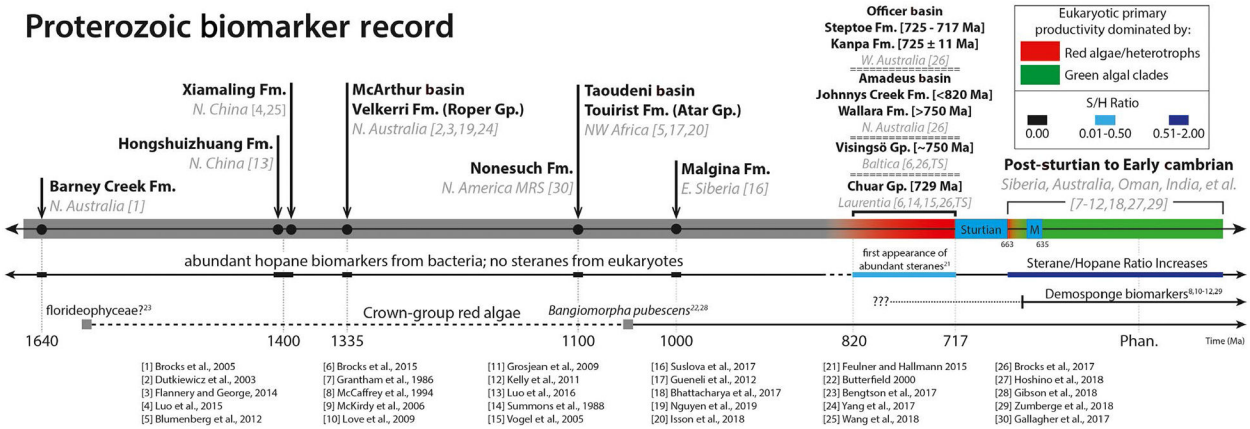

FIGURE 1.

Composite ancient biomarker timeline record compiled using extractable sedimentary organic matter from rocks deposited through the Mesoproterozoic and into the early Phanerozoic, depicting the ecological expansion of steroid-producing eukaryotes as they became more abundant relative to bacteria. Regular (4-desmethyl) steranes first appear in the rock record between ca. 820 and 720 Ma (Brocks et al., 2017; Isson et al., 2018; this study) causing the first substantial step increase in the S/H ratio, suggestive of an algal rise, in the late Tonian Period. A switch in the dominant eukaryotic primary producers, from a C_{27} (red shaded area for red algae) to a C_{29} (green shaded area for green algae) sterane dominance, differentiates pre- and post-Sturtian marine paleoenvironments, respectively. From ca. 660–635 Ma (Rooney et al., 2014), C_{30} demosponge steranes (24-ipc and 26-mes; Love et al., 2009; Zumberge et al., 2018) are first detected during the Cryogenian interglacial period. Timeline updated from Isson et al. (2018)

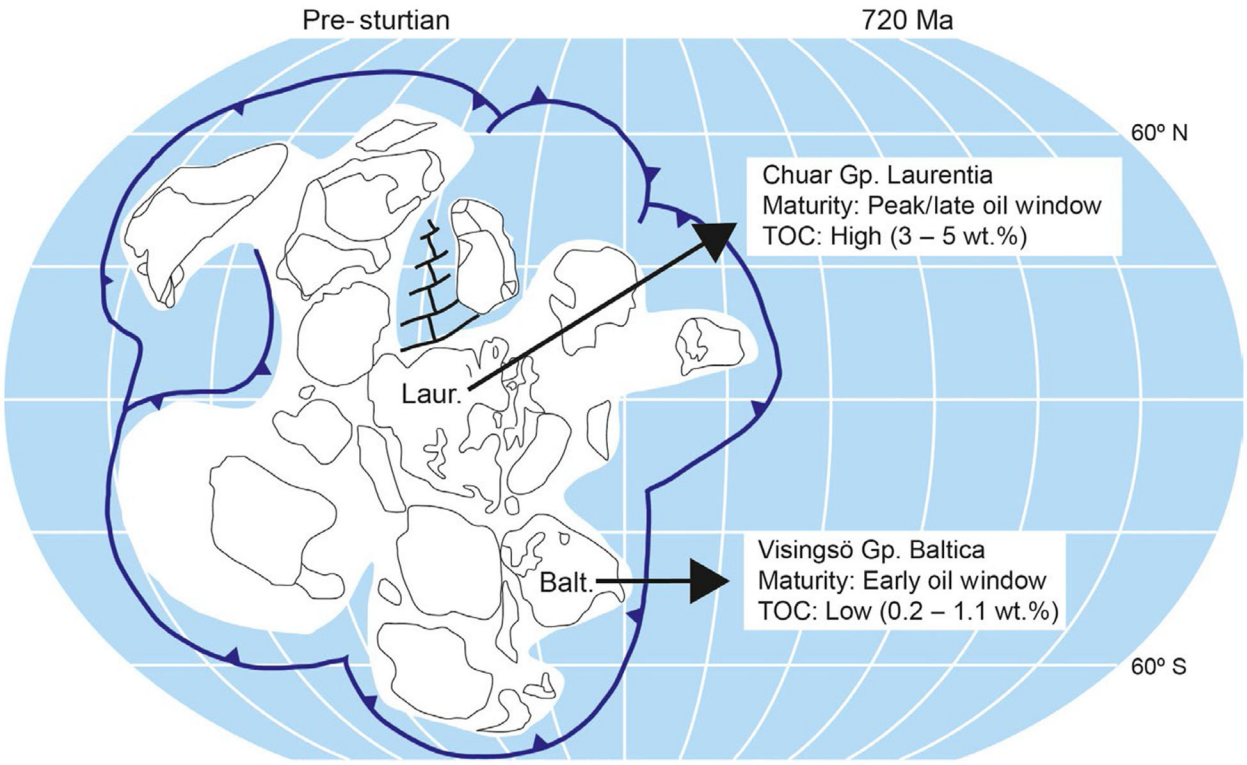

FIGURE 2.

Tonian paleography highlighting the locations of two paleocontinents, Laurentia (Laur.) and Baltica (Balt.), from where the Chuar Group and Visingsö Group samples were originally deposited offshore, respectively. Differences in thermal maturity and TOC content are observed across the sample set. Map adapted and modified from Hoffman et al. (2017)

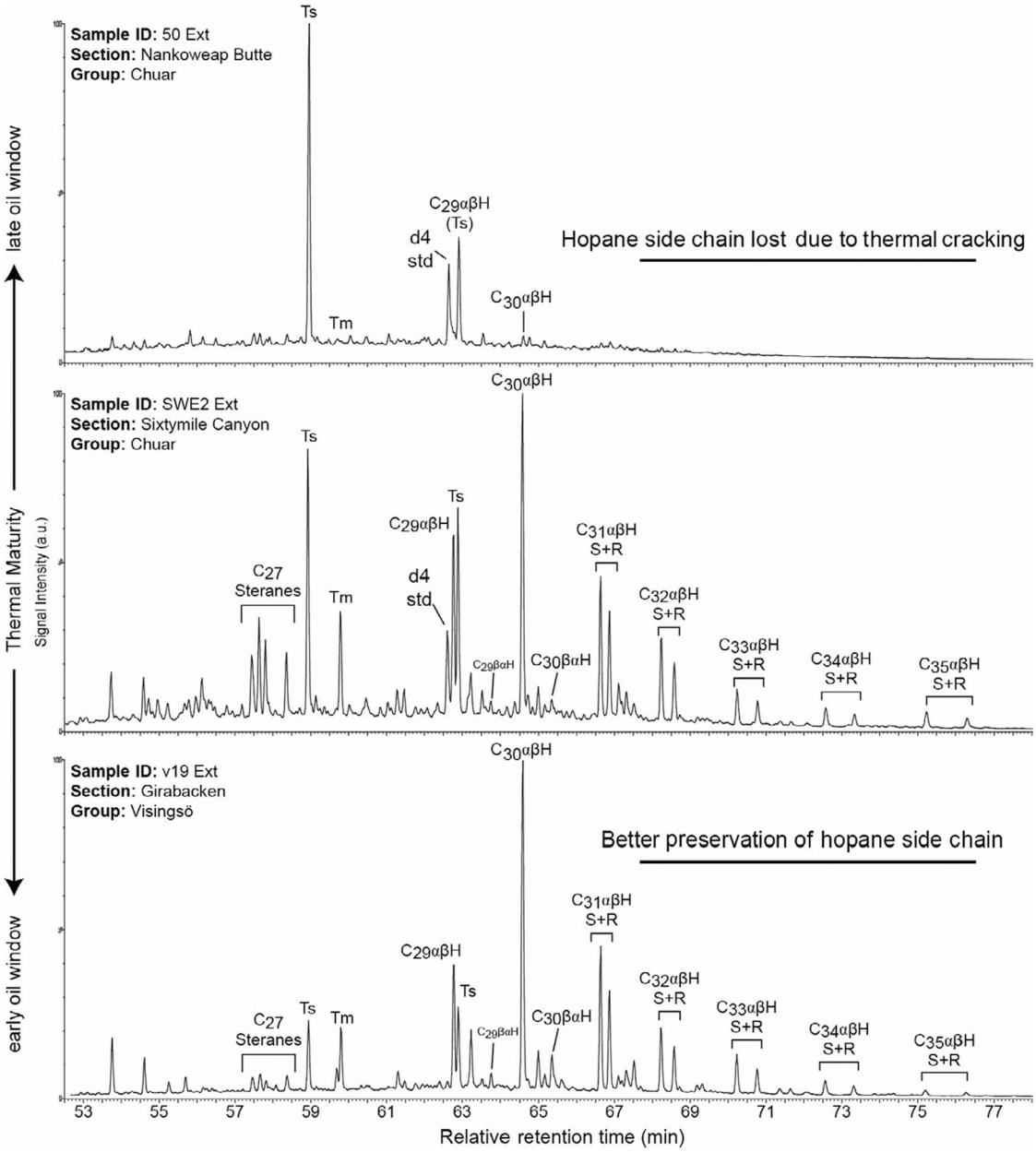

FIGURE 3.

C_{26}–C_{30} sterane and C_{27}–C_{35} hopane distributions from composite chromatograms (MRM-GC-MS transitions $M^+ \rightarrow 217 + 191$) of the free (extractable) organic matter highlight thermal maturity differences between the samples used in this study. Rocks from the Walcott Member of the Chuar Group are either (top) *late* oil window maturity, characteristic of the Nankoweap Butte section or (middle) of *peak* oil window maturity, characteristic of the Sixtymile Canyon locality. Conversely, rocks recovered from all sections in the Visingsö Group are less mature and of (bottom) intermediate *early–middle* oil window maturity, consistent with the compound distributions. See Table 2 footnote for peak identifications

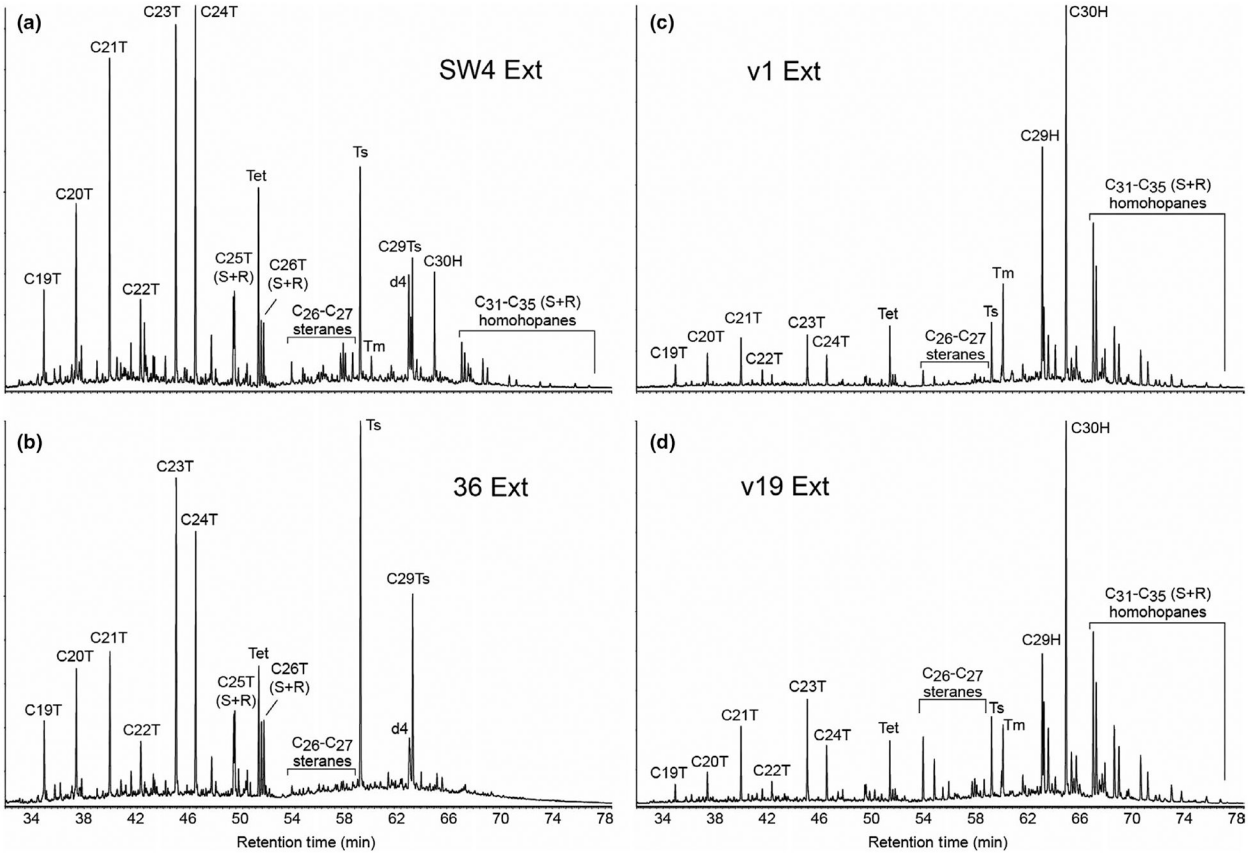

FIGURE 4.

Composite MRM-GC-MS traces of polycyclic biomarker alkanes for representative solvent-extractable biomarker profiles from the (a, b) Chuar and (c, d) Visingsö Groups. Biomarker hydrocarbon distributions (e.g., tricyclic terpanes, hopanes, and steranes) are influenced by source biota, depositional environment, and the thermal maturity of the host rock. See Table 2 for a suite of biomarker ratios calculated using peak area integration

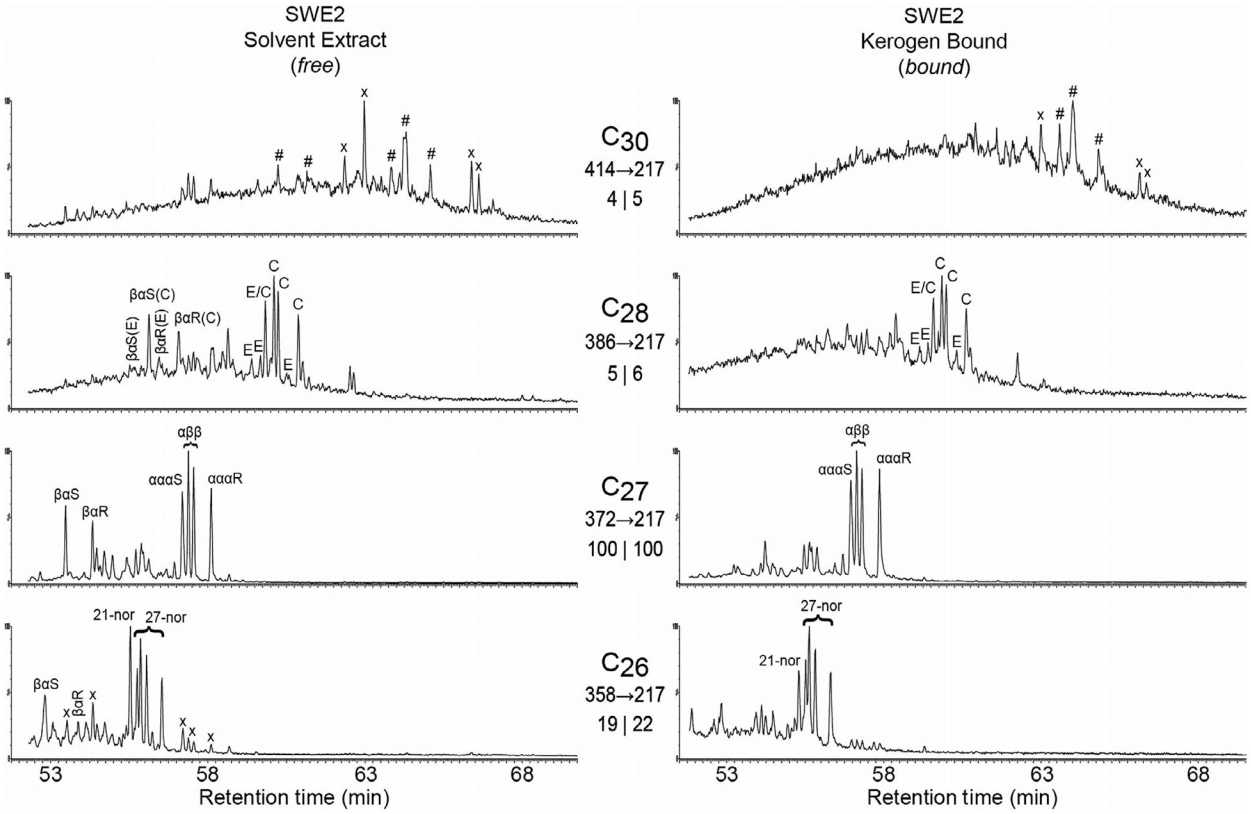

FIGURE 5.

MRM-GC-MS ($M^+ \rightarrow 217$ Da) chromatograms of the *free* (left) and *kerogen-bound* (right) C_{26}–C_{30} steranes from sample SWE2 (Chuar Group, Sixtymile Canyon locality). Sterane distributions and relative abundance comparisons between the bitumen and kerogen phases of sedimentary organic matter confirm that the biomarkers are syngenetic with the host sedimentary rocks. Compared to the *free* phase, the sterane distributions from the *bound* phase show a slightly less mature compound distribution (e.g., 21-nor < 27-nor, C_{27} ααaR > ααaS) due to steric protection from the kerogen network. The "regular" sterane series show the four stable isomer peaks (the ααaS + R and αββR + S isomers), while "βαS" and "βαR" indicate the two main diasterane isomers, which are rearranged steranes prominent in the free biomarker distributions. 21-nor = 21-norcholestane; 27-nor = 27-norcholestane; E = ergostane; C = cryostane; # = C_{30} series with unknown side chain chemistry. Cross talk (x) from the more abundant hopanes can appear in the C_{30} sterane (414→217 Da) trace when C_{30} sterane abundances are low/absent

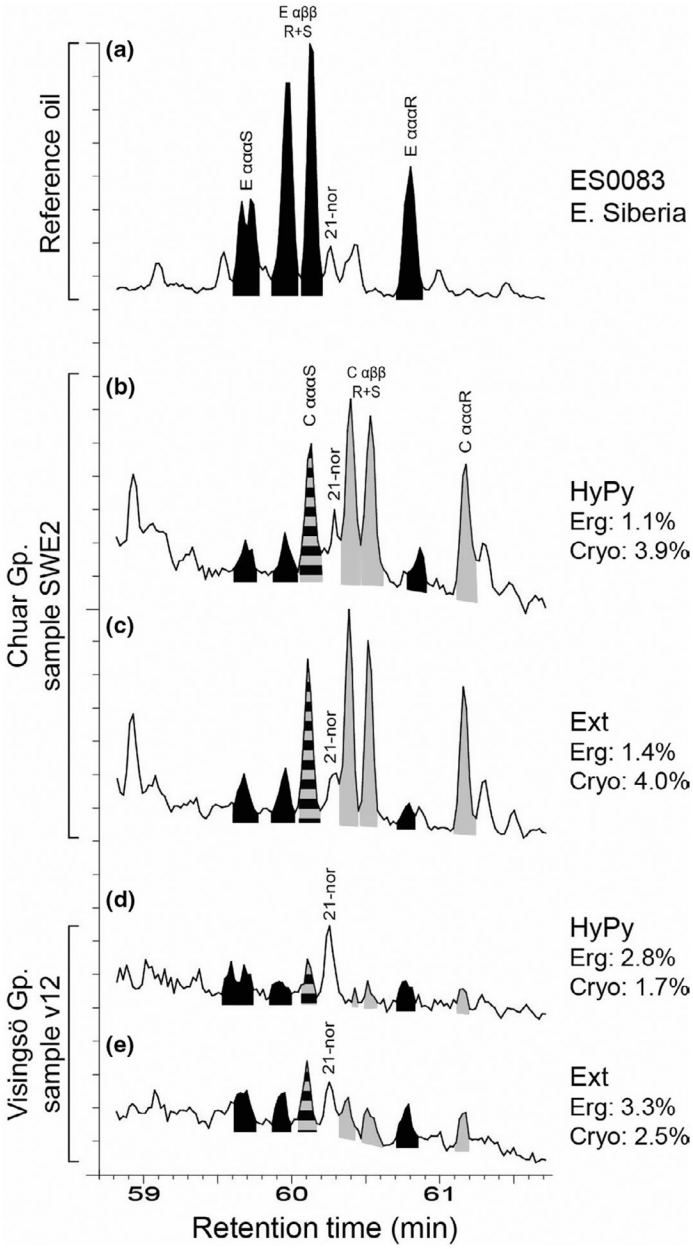

FIGURE 6.

MRM-GC-MS (386→217 Da) chromatograms of the C_{28} sterane distributions from the *kerogen-bound* (HyPy) and *solvent-extractable* (Ext) biomarker pools from representative samples from the Chuar Group (b and c) and Visingsö Group (d and e). The abundances of ergostane (Erg) and cryostane (Cryo) in each sample, relative to the total detectable C_{26}–C_{30} steranes, are shown on the right (as % of total). Cryostane is negligible in (a) ES0083 Lower Cambrian Reference Oil from Eastern Siberia (Kelly, Love, Zumberge, & Summons, 2011) but present in the Tonian rocks (b–e). Black shaded peaks = ergostane (ααaS + R and αββR + S isomers) = E; Gray shaded peaks = cryostane (ααaS + R and αββR + S isomers) = C; Striped peak = co-elution of αββ 20(S) ergostane and aaa 20(S) cryostane; 21-nor = 21-norstigmastane

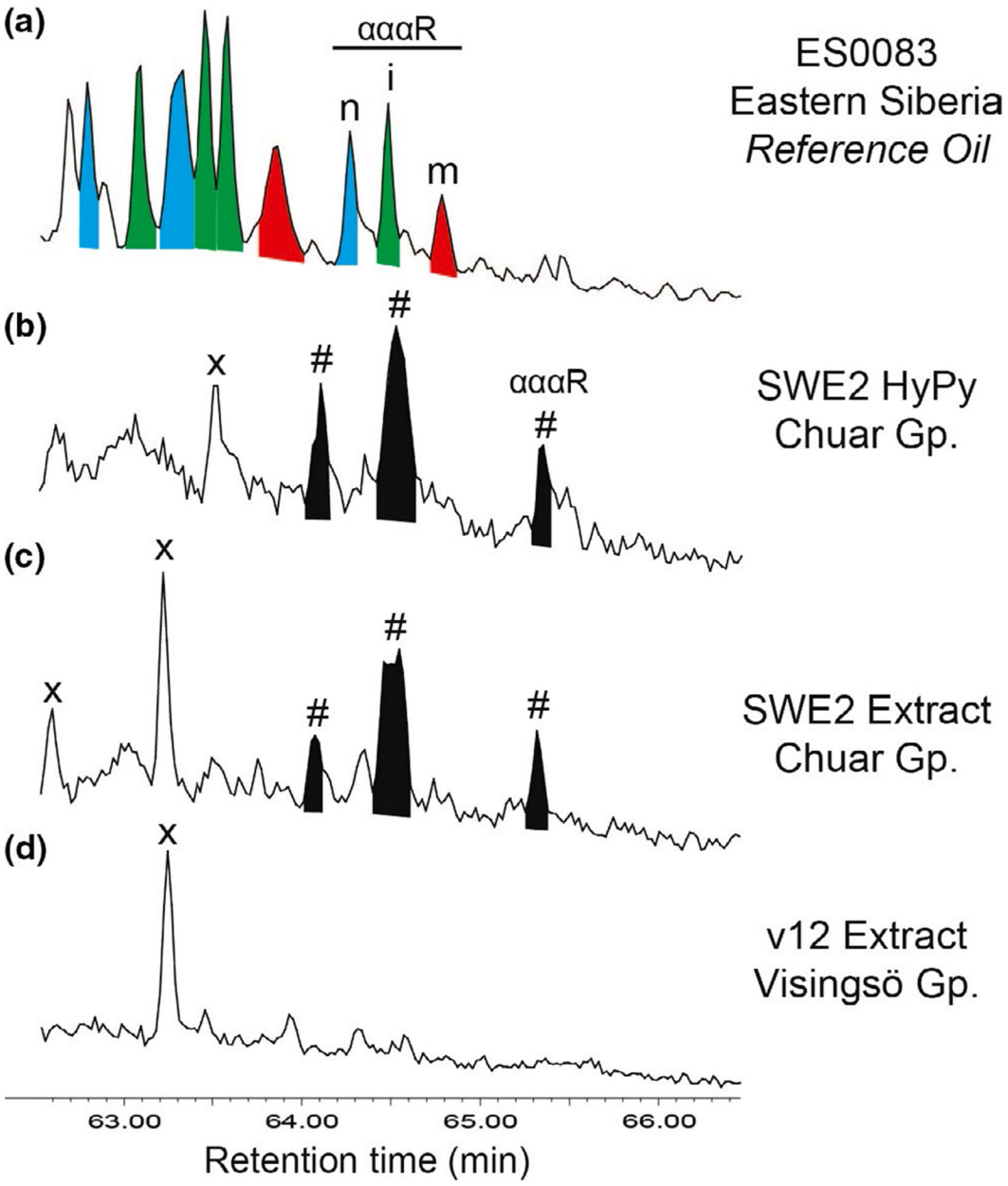

FIGURE 7.

MRM-GC-MS (414→217 Da) chromatograms of the C_{30} sterane distributions in representative Tonian sedimentary rocks (b-c, this study) compared with a (a) ES0083 Lower Cambrian Reference Oil from Eastern Siberia (Kelly et al., 2011). ES0083 has a C_{30} sterane distribution with three different resolvable series: 24-*n*-propylcholestane (n/blue peaks), 24-isopropylcholestane (i/green peaks), and 26-methylstigmastane (m/red peaks; Love et al., 2009; Zumberge et al., 2018). One novel C_{30} sterane series (#/black peaks) was detected in the least mature rocks of the Chuar Group from Sixtymile Canyon section. The new C_{30} sterane series is found in the (c) solvent extract (*free*) phase of sample SWE2 and also in the (b) kerogen (*bound*) phase. Sample (d) v12 shows the absence of any detectable C_{30} steranes within the Visingsö Group outcrops. Peaks labeled "X" represent cross talk

from other compound classes (usually hopanes). The ααα*R* isomer is indicated by a label to show the difference in compound elution times between all four C_{30} sterane series (in increasing elution order of 24-npc, 24-ipc, 26-mes with the new C_{30} sterane compound eluting last)

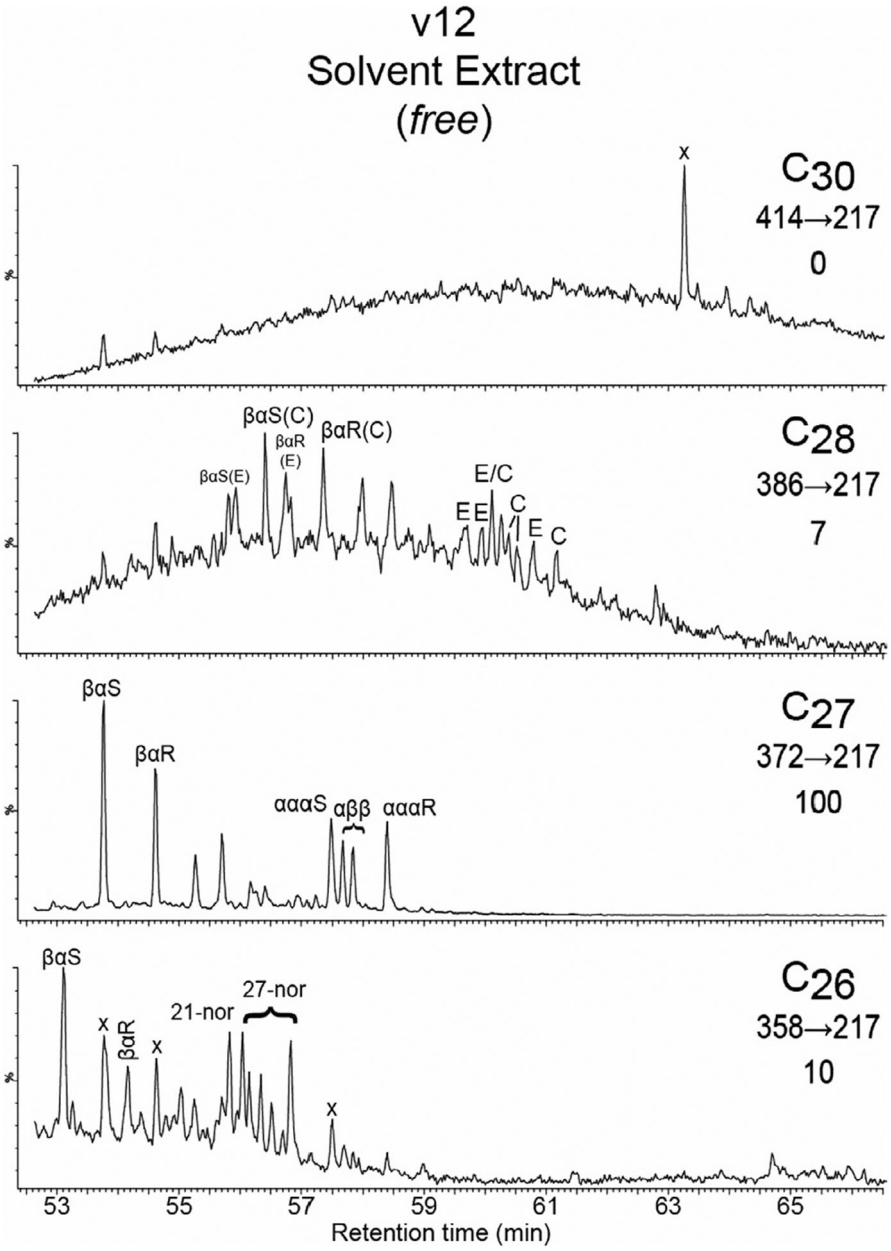

FIGURE 8.

MRM-GC-MS ($M^+ \rightarrow 217$ Da) chromatograms of the extractable (*free*) C_{26}–C_{30} steranes from sample v12 (Visingsö Group, Broken Nodule). There are at least four detectable "regular" sterane series (each with ααα S, αββR, αββS, αααR isomers). 21-nor = 21-norcholestane; 27-nor = 27-norcholestane; E = ergostane; C = cryostane. Cross talk (x) peaks from hopanes are dominant in the C_{30} (414→217 Da) chromatogram since C_{30} sterane abundances are trace/absent for Visingsö samples

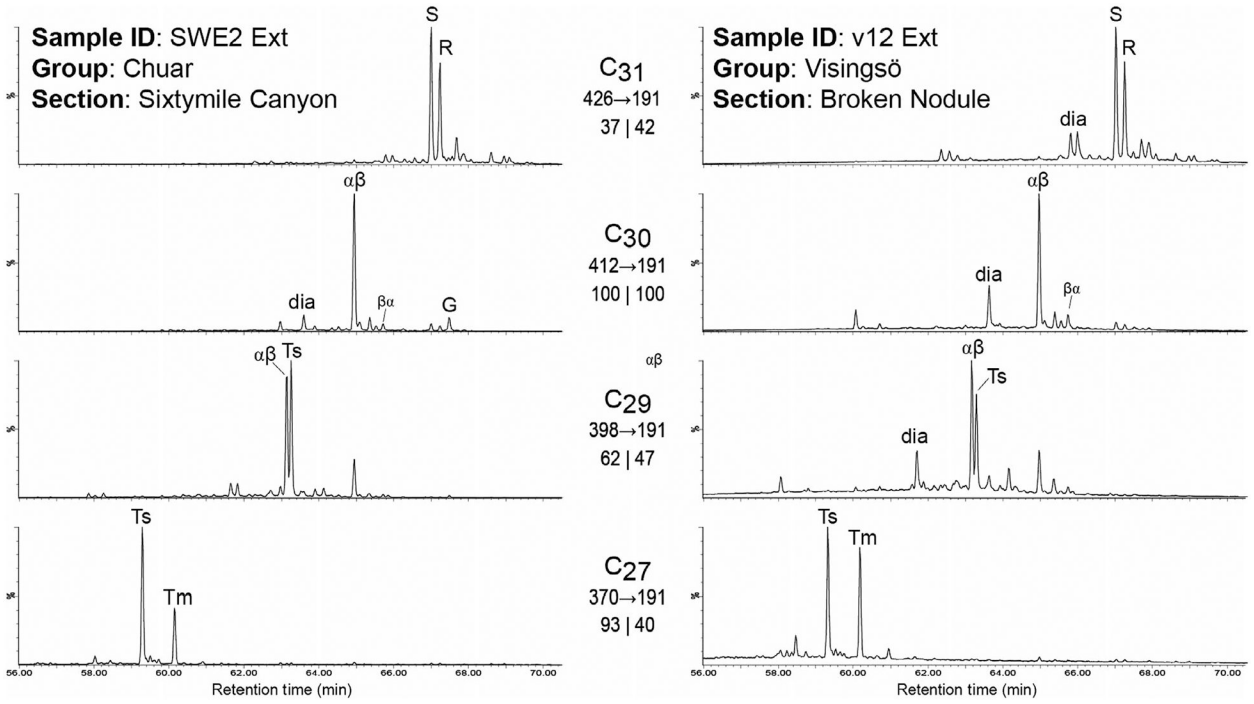

FIGURE 9.

MRM-GC-MS ($M^+ \rightarrow 191$ Da) chromatograms of the C_{27}–C_{31} hopanes for samples (left) SWE2 from the Walcott Member of the Chuar Group and (right) v12 from the Visingsö Group. Differences in the thermal history for each sample are reflected by key hopane compound ratios: C_{27} Ts/Tm; C_{29} Ts/αβH; C_{30} βαH/αβH. The Chuar Group has higher amounts of gammacerane (G) relative to hopanes, while the Visingsö Group has elevated diahopanes (dia), reflecting some differences in microbial ecologies and environmental conditions. Relative abundances (from % of signal intensity) for each trace are shown beneath the MRM mass transition ($M^+ \rightarrow 191$ Da), with C_{30} hopanes being most abundant (100%)

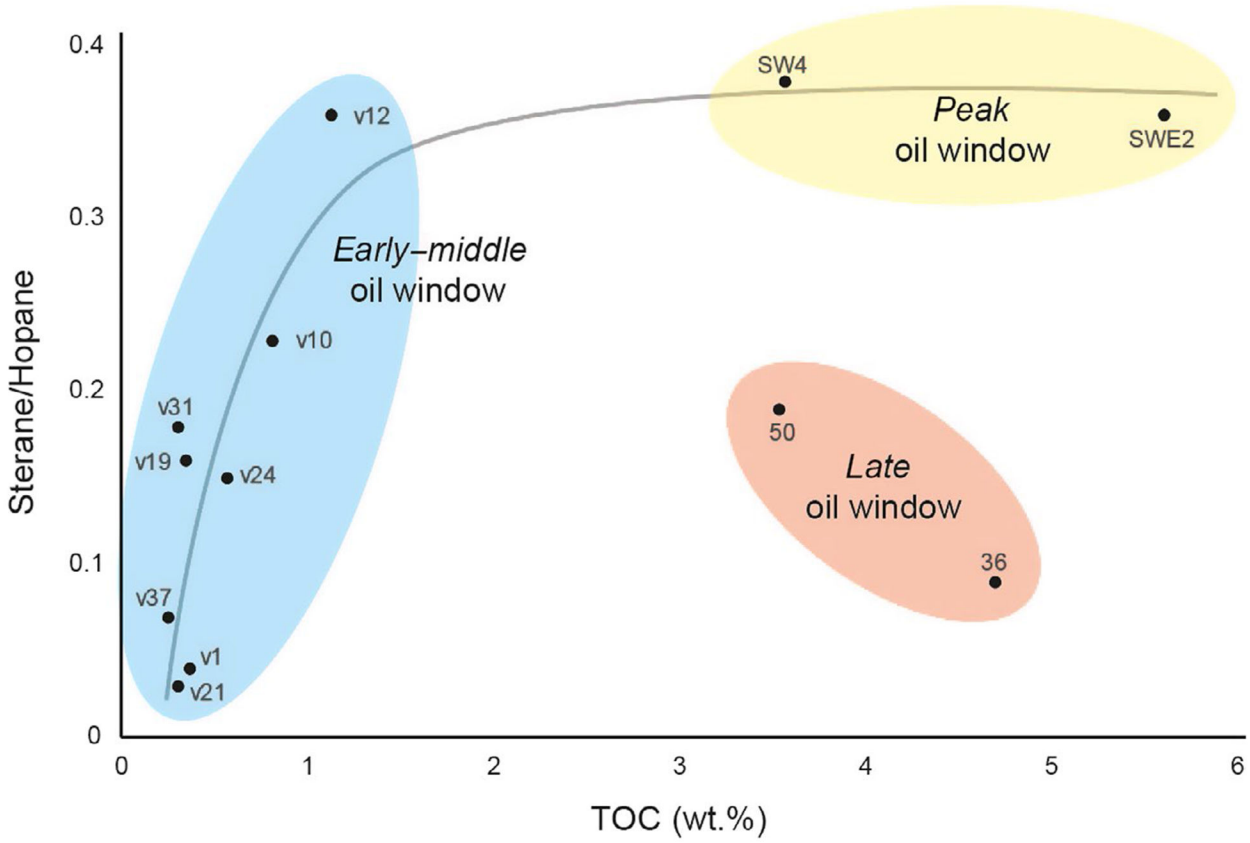

FIGURE 10.

Comparison of Total Organic Carbon (TOC) content of rocks versus Sterane/Hopane (S/H) ratio as measured from MRMGC-MS from the conventional solvent-extractable (*free*) organic phase. Samples from the Visingsö Group fall within the *early–middle* oil window (blue shaded area) with TOC values between 1.13 and 0.26 wt.%. Generally, the more organic-rich samples show higher S/H ratios, consistent with an enhanced eukaryotic source contribution in more productive and nutrient-replete Neoproterozoic marine settings. A maturity gradient exists within the organic-rich Chuar Group samples (5.61–3.54 wt.% TOC), with the *late* oil window samples from Nankoweap Butte outcrop locality (orange shaded area) generating lower S/H values falling off-trend compared to the less mature *peak* oil window (yellow shaded area) samples. The less mature Chuar samples (yellow shaded area) from the Sixtymile Canyon locality are more likely to preserve a biomarker signal closer to the original S/H values due to a lower extent of side chain cleavage and other thermal cracking, aromatization, and rearrangement reactions during burial maturation

TABLE 1

Total Organic Carbon (TOC) contents and Rock-Eval pyrolysis parameters for rocks used

Section/locality	Sample ID	TOC (wt.%)	S2 (mg HC/g)	HI(mg/gTOC)	T_{max} (°C)
Chuar Gp., Kwagunt Fm., Walcott Mbr. (Grand Canyon, AZ, USA)					
Nankoweap Butte	36	4.70	4.13	88	437[a]
	50	3.54	2.27	64	436[a]
Sixtymile Canyon	SW4	3.57	4.25	119	439
	SWE2	5.61	7.39	132	444
Visingsö Gp., Upper Fm. (Lake Vättern, South Central Sweden)					
Uppgranna	v1	0.37	0.22	60	442
Broken Nodule	v10	0.82	1.44	176	432
	v12	1.13	2.54	225	433
	v24	0.57	0.75	132	432
	v31	0.31	0.37	120	438
	v37	0.26	0.28	107	439
Girabacken	v19	0.35	0.43	124	440
Boeyrd	v21	0.31	0.30	97	433

Note: TOC (wt.%) = total organic carbon; S2 (mg HC/g) captured at a high ramp temperature [~430–460°C] = mass of hydrocarbons (HC) that are measured from fragmentation of labile kerogen during thermal pyrolysis of the sample; HI (Hydrogen Index, mg/g TOC) = S2 × 100/TOC; T_{max} values are pyrolysis temperatures at which S2 peaks yield maximum signal.

[a]These are the two most mature rocks in our sample set from molecular maturity assessment for which T_{max} values are suspiciously low. The errors in T_{max} determination are greater for high maturity samples due to low intensity and/or broad asymmetrical S2 peak profiles, which often leads to under-estimation of maturity.

TABLE 2

Maturity and source sensitive biomarker ratios from the solvent extract (SE) and kerogen-bound (KB) phases of organic matter

Location	**Chuar group**								**Visingsö group**									
Section	**Nankoweap Butte**				**Sixtymile Canyon**				**Broken Nodule**						**Upg**	**Girabacken**		**Byd**
Sample ID	**36**		**50**		**SW4**		**SWE2**		**v1O**	**v12**		**v24**	**v31**	**v37**	**v1**	**v19**		**v21**
Free (SE)/Bound (KB)	**SE**	**KB**	**SE**	**KB**	**SE**	**KB**	**SE**	**KB**	**SE**	**SE**	**KB**	**SE**	**SE**	**SE**	**SE**	**SE**	**KB**	**SE**
Hopane distributions																		
Maturity sensitive																		
Tricyclics/$C_{30}\alpha\beta$H	191	77	170	239	14	96	5.8	8.7	2.7	2.6	48	2.2	1.5	1.0	0.6	0.8	7.1	0.7
C_{27} Ts/Tm	214	2.68	111	1.71	8.99	0.15	2.39	0.07	1.30	1.17	0.04	1.46	0.86	0.44	0.58	1.07	0.04	0.46
C_{29} Ts/apH	7.10	0.66	7.13	0.49	1.86	0.07	1.09	0.09	0.80	0.76	0.02	1.08	0.56	0.34	0.31	0.63	0.03	0.24
30-norH/$C_{30}\alpha\beta$H	2.52	0.25	0.98	0.24	0.11	0.13	0.08	0.14	0.06	0.06	0.10	0.05	0.04	0.06	0.04	0.03	0.04	0.05
$C_{30}\beta\alpha$H/$C_{30}\alpha\beta$H	0.00	0.25	0.00	0.08	0.05	0.09	0.05	0.06	0.12	0.13	0.34	0.10	0.12	0.14	0.10	0.09	0.32	0.12
$C_{31}\alpha\beta$H 22S/(S + R)	0.51	0.47	0.54	0.50	0.56	0.57	0.57	0.59	0.57	0.56	0.54	0.56	0.58	0.57	0.57	0.58	0.60	0.58
Source sensitive																		
Tet/C_{23}T	0.30	0.35	0.24	0.24	0.42	0.14	0.43	0.20	0.27	0.29	0.32	0.24	0.24	0.70	0.84	0.42	0.48	1.38
C_{26}T/C_{25}T	1.02	1.04	1.05	0.87	0.77	0.85	0.74	1.00	1.09	0.99	0.95	1.29	0.73	1.21	1.36	0.78	1.07	0.97
$C_{29}\alpha\beta$H/$C_{30}\alpha\beta$H	4.05	1.58	1.43	1.82	0.55	2.60	0.54	1.89	0.49	0.43	4.43	0.41	0.41	0.55	0.64	0.38	3.00	0.65
G/$C_{30}\alpha\beta$H	0.30	0.21	0.27	0.22	0.19	0.45	0.11	0.15	0.03	0.03	n.d.	0.04	0.07	0.01	0.02	0.03	0.02	0.01
2α MeH/3pMeH	n.d.	n.d.	1.13	n.d.	0.24	0.50	0.13	0.38	0.40	0.39	3.65	0.36	0.43	0.52	0.67	0.34	1.33	0.36
Sterane/Hopane ratios																		
Sterane/Hopane (1)	0.09	0.56	0.19	1.01	0.38	1.26	0.37	0.36	0.23	0.36	0.37	0.15	0.18	0.07	0.04	0.16	0.16	0.03
S/H (2)	0.05	0.38	0.11	0.69	0.27	0.81	0.28	0.28	0.20	0.32	0.30	0.13	0.17	0.06	0.04	0.15	0.15	0.03
S/H (3)	0.04	0.27	0.10	0.41	0.22	0.46	0.23	0.23	0.16	0.24	0.23	0.12	0.14	0.06	0.04	0.13	0.13	0.03
Sterane distributions																		
%C_{26}	40	32	38	32	23	29	17	17	12	8	15	9	4	6	3	4	7	2
%C_{27}	49	68	53	68	70	63	76	76	80	86	80	80	89	82	86	91	88	98
%C_{28} (Erg)	7	n.d.	5	n.d.	2	2	1	1	5	3	3	6	4	8	8	3	3	n.d.
%C_{28} (Cryo)	4	n.d.	4	n.d.	4	4	4	4	4	3	2	5	3	4	3	2	2	n.d.
%C_{28} (total)	11	n.d.	9	n.d.	6	6	5	5	9	6	5	11	7	12	11	5	5	n.d.

Location	Chuar group								Visingsö group									
Section	Nankoweap Butte				Sixtymile Canyon				Broken Nodule						Upg	Girabacken		Byd
Sample ID	36		50		SW4		SWE2		v1O	v12		v24	v31	v37	v1	v19		v21
Free (SE)/Bound (KB)	SE	KB	SE	KB	SE	KB	SE	KB	SE	SE	KB	SE	SE	SE	SE	SE	KB	SE
%C_{30} (unknown)	n.d.	n.d.	n.d.	n.d.	1	2	1	2	n.d.	n.d.	n.d.	n.d.	n.d.	n.d.	n.d.	n.d.	n.d.	n.d.
Cryo/Chol	0.08	n.d.	0.07	n.d.	0.06	0.07	0.05	0.05	0.04	0.03	0.02	0.06	0.03	0.05	0.04	0.02	0.02	n.d.
Dia/Reg C_{27}	1.43	<0.04	0.79	<0.02	0.31	<0.01	0.31	<0.01	1.64	1.02	<0.03	1.42	1.45	1.11	1.40	1.57	<0.04	1.14

Note: Upg: Uppgranna; Byd: Boeyrd; Tricyclics: C_{19}–C_{26} tricyclic terpanes; $C_{30}\alpha\beta$H: 17α(H),21β(H)-hopane; C_{27}Ts: 18α(H)-trisnorneohopane; C_{27}Tm: 17α(H)-trisnorhopane; C_{29}Ts: 18α−30-norneohopane; $C_{29}\alpha\beta$H: 17α(H),21β(H)-30-norhopane; 30-norH: 17α(H),21β(H)-30-norhomohopane; $C_{30}\beta\alpha$H: 17β(H),21α(H)-hopane (moretane); $C_{31}\alpha\beta$H: 17α(H),21β(H)-homohopane (S & R denote stereochemistry at the C-22 position); Tet: C_{24} tetracyclic terpane; C_{23}T: C_{23} tricyclic terpane; C_{26}T: C_{26} tricyclic terpane; C_{25}T: C_{25} tricyclic terpane; G: gammacerane; 2αMeH: 2α-methylhopane; 3βMeH: 3β-methylhopane; S/H (1) as defined in this study: Σ(dia- + regular C_{26}–C_{30} steranes [includes cryostanes and the unknown C_{30} series])/Σ(C_{27}–C_{35} αβ hopanes); S/H (2) from Brocks et al. (2017): Σ(dia- + regular C_{27}–C_{29} steranes [excludes C_{26} norcholestanes and cryostanes])/Σ(C_{27}–C_{35} αβ hopanes); S/H (3) from Brocks et al. (2015): Σ(dia- + regular cholestanes and cryostanes [excludes C_{26} norcholestanes and ergostanes]/Σ(C_{27}–C_{35} αβ hopanes); Cryo (cryostane): 26-methylcholestane; Chol: cholestane; Erg: ergostane; Dia/Reg C_{27}: βα−20(S + R)-diacholestanes/[ααα- and αββ−20(S + R)-regular cholestanes]; n.d.: not detectable. All ratios are derived from MRM-GC-MS analyses.